

Discovery and Preclinical Characterization of 3-((4-(4-chlorophenyl)-7-fluoroquinoline-3-yl)sulfonyl)benzotrile, a Novel Non-acetylenic Metabotropic Glutamate Receptor 5 (mGluR5) Negative Allosteric Modulator for Psychiatric Indications

János Galambos, Attila Bielik, Mikhail Krasavin, Zoltán Orgován, György Domány, Katalin Nógrádi, Gábor Wágner, György T. Balogh, Zoltán Béni, János Koti, Zoltán Szakács, Amrita Bobok, Sándor Kolok, Mónika L. Miko-Bakk, Mónika Vastag, Katalin Sággy, Judit Laszy, Attila Sándor Halász, Ottilia Balázs, Krisztina Gál, István Greiner, Zsolt Szombathelyi, and György M Keser#

J. Med. Chem., **Just Accepted Manuscript** • DOI: 10.1021/acs.jmedchem.6b01858 • Publication Date (Web): 17 Feb 2017

Downloaded from <http://pubs.acs.org> on February 18, 2017

Just Accepted

“Just Accepted” manuscripts have been peer-reviewed and accepted for publication. They are posted online prior to technical editing, formatting for publication and author proofing. The American Chemical Society provides “Just Accepted” as a free service to the research community to expedite the dissemination of scientific material as soon as possible after acceptance. “Just Accepted” manuscripts appear in full in PDF format accompanied by an HTML abstract. “Just Accepted” manuscripts have been fully peer reviewed, but should not be considered the official version of record. They are accessible to all readers and citable by the Digital Object Identifier (DOI®). “Just Accepted” is an optional service offered to authors. Therefore, the “Just Accepted” Web site may not include all articles that will be published in the journal. After a manuscript is technically edited and formatted, it will be removed from the “Just Accepted” Web site and published as an ASAP article. Note that technical editing may introduce minor changes to the manuscript text and/or graphics which could affect content, and all legal disclaimers and ethical guidelines that apply to the journal pertain. ACS cannot be held responsible for errors or consequences arising from the use of information contained in these “Just Accepted” manuscripts.

1
2
3
4
5
6
7
8
9
10
11
12
13
14
15
16
17
18
19
20
21
22
23
24
25
26
27
28
29
30
31
32
33
34
35
36
37
38
39
40
41
42
43
44
45
46
47
48
49
50
51
52
53
54
55
56
57
58
59
60

Discovery and Preclinical Characterization of 3-((4-(4-chlorophenyl)-7-fluoroquinoline-3-yl)sulfonyl)benzotrile, a Novel Non-acetylenic Metabotropic Glutamate Receptor 5 (mGluR5) Negative Allosteric Modulator for Psychiatric Indications

János Galambos,¹ Attila Bielik,¹ Mikhail Krasavin,² Zoltán Orgován,³ György Domány,^{1*} Katalin Nógrádi,¹ Gábor Wágner,¹ György T. Balogh,¹ Zoltán Béni,¹ János Kóti,¹ Zoltán Szakács,¹ Amrita Bobok,¹ Sándor Kolok,¹ Mónika L. Mikó-Bakk,¹ Mónika Vastag,¹ Katalin Sággy,¹ Judit Laszy,¹ Attila Sándor Halász,¹ Ottilia Balázs,¹ Krisztina Gál,¹ István Greiner,¹ Zsolt Szombathelyi,¹ György M. Keserű^{3*}

Gedeon Richter Plc, 19-21 Gyömrői út, Budapest, 1103 Hungary

*Institute of Chemistry, Saint Petersburg State University, 26 Universitetskii Prospekt, Peterhof 198504
Russia*

Medicinal Chemistry Research Group, Research Centre for Natural Sciences, Hungarian Academy of Sciences, 2 Magyar tudósok körútja, Budapest, 1117 Hungary.

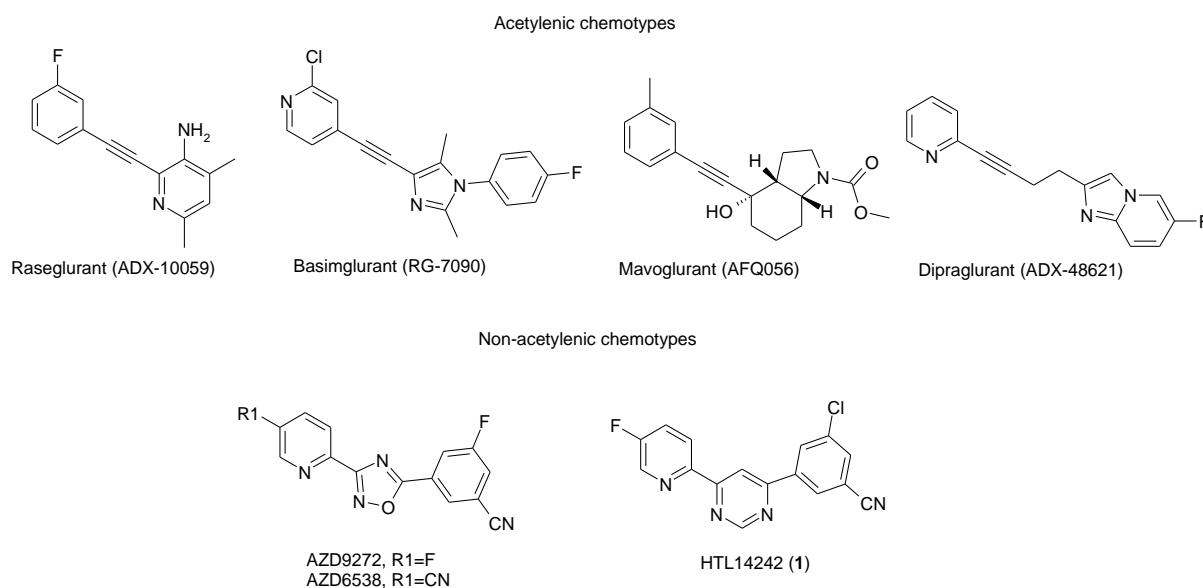
Abstract

Negative allosteric modulators (NAM) of metabotropic glutamate receptor 5 (mGluR5) have been implicated as potential pharmacotherapy for a number of psychiatric diseases including anxiety and depression. Most of the mGluR5 NAM clinical candidates can be characterized by the central acetylenic moiety that connects the terminal pharmacophores. Identification of a sulfoquinoline hit *via* high throughput screening (HTS) followed by optimization provided a 4-phenyl-3-aryl-sulfoquinoline lead compound with the minimal pharmacophore. Optimization of the core and aryl appendages was

1
2
3 performed by scanning and matrix libraries synthesized by the multiple parallel synthesis approach.
4
5 Biological evaluation of matrix libraries provided a number of potent, metabolically stable and *in vivo*
6
7 active compounds. One of these compounds, **25** showed high efficacy and safety in preclinical *in vivo*
8
9 models this allowed its nomination as a novel, non-acetylenic mGluR5 NAM clinical candidate.
10
11
12 Compound **25** was advanced to first-in-man trials for the treatment of psychiatric conditions.
13
14
15
16
17
18

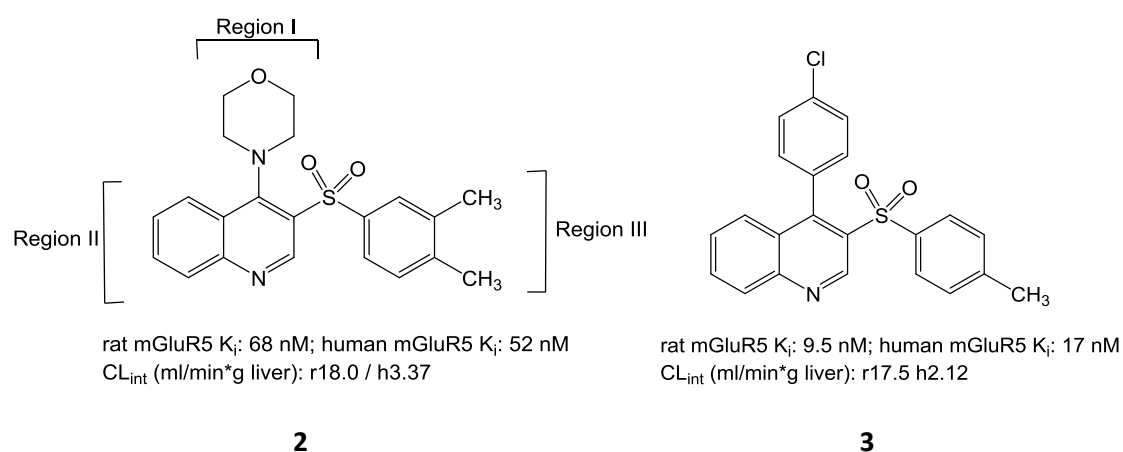
19 Introduction

20
21 Metabotropic glutamate receptors (mGluRs) constitute the class C of G-protein coupled receptors
22
23 (GPCRs) and play a key role in glutamatergic signaling.¹ This class of GPCRs consists of three subclasses
24
25 including groups I (mGluR1 and mGluR5), II (mGluR2 and mGluR3), and III (mGluR4, mGluR6, mGluR7
26
27 and mGluR8). Group I mGluRs are Gq coupled, located mainly postsynaptically and their activation
28
29 increases NMDA receptor activity and neuronal excitability. The inhibition of mGluR5 which is mostly
30
31 expressed in the striatum, hippocampus, amygdala, and frontal cortex is therefore considered as a
32
33 potential therapeutic intervention in a number of psychiatry indications including fragile X syndrome,²
34
35 anxiety,³ and depression.⁴ Due to the indirect enhancement of NMDA activity mGluR5 activators might
36
37 be effective in schizophrenia,⁵ can improve cognitive⁶ and memory performance.⁷ Since the orthosteric
38
39 glutamate site is highly conserved for all the mGluRs, most of the discovery programs are directed
40
41 toward allosteric modulators that would provide the necessary selectivity not only between but also
42
43 within the subclasses.⁸ In the case of mGluR5 these approaches yielded different chemotypes as
44
45 negative and positive allosteric modulators (NAMs and PAMs, respectively). Early mGluR5 NAMs were
46
47 rod-like compounds where terminal rings were connected typically by an acetylenic moiety. In fact,
48
49 compounds that reached the clinic up to now (ADX-10059,⁹ RG-7090,¹⁰ AFQ056¹¹ and ADX-48621¹²) all
50
51 belong to this class of compounds (Figure 1). In more recent mGluR5 NAM chemotypes the terminal
52
53 rings are connected by 5- or 6-membered heterocycles as exemplified by AZD6538 and AZD9272¹³ and
54
55 HTL14242¹⁴ (**1**) clinical candidates (Figure 1).
56
57
58
59
60



23 Figure 1. Clinical mGluR5 NAMs of acetylenic and non-acetylenic chemotypes

24
25
26
27
28 As a part of our research program for searching novel non-acetylenic chemotypes we identified a
29 morfolino-sulfoquinoline derivative (**2**) by screening our corporate compound deck (Figure 2).¹⁵ Based
30 on our previous experience with thieno[2,3-b]pyridines^{16,17} the original hit (**2**) was rapidly converted
31 to the 4-chlorophenyl derivative (**3**) in Region I, this showed improved potency but virtually the same
32 low metabolic stability in both rat and human microsomes (Figure 2).
33
34
35
36
37
38



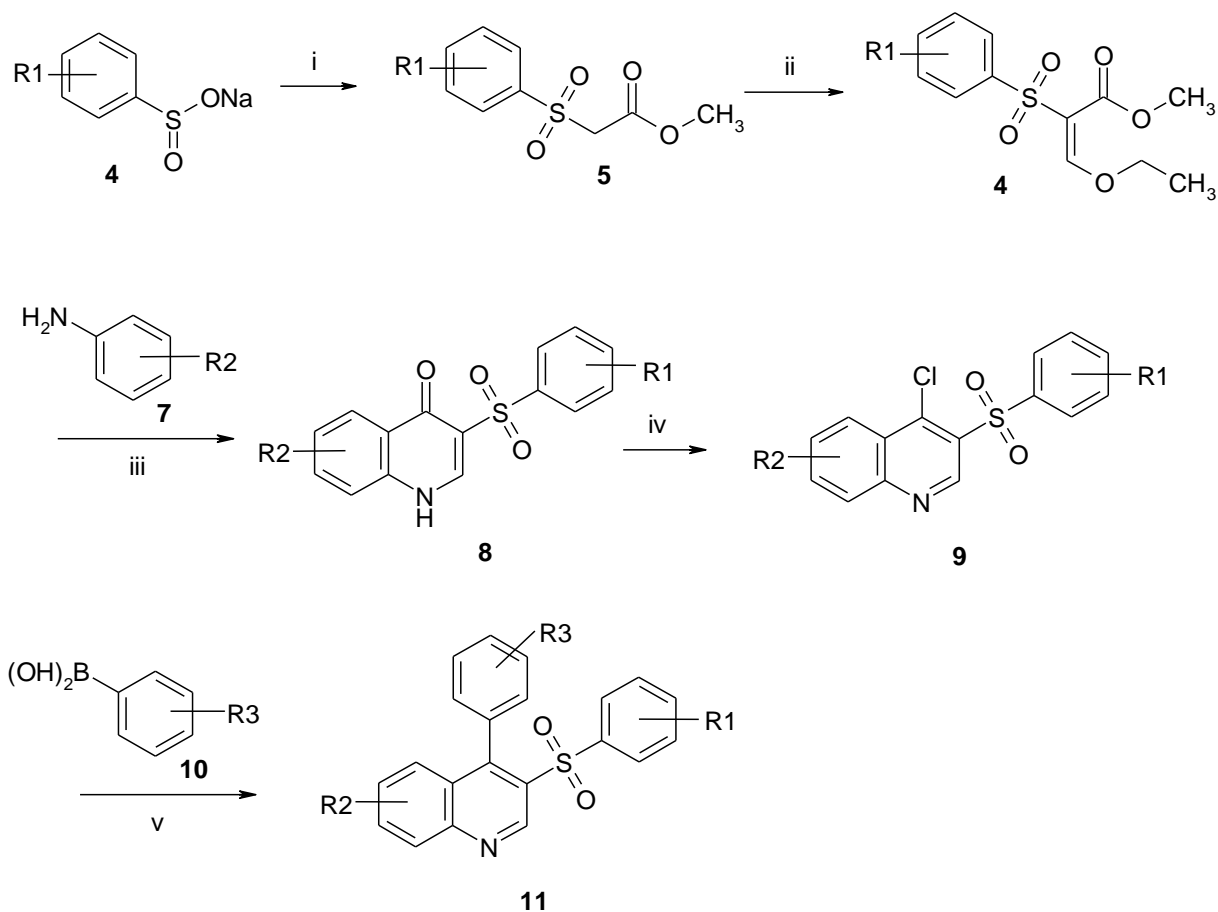
54 Figure 2. The amino-sulfoquinoline HTS hit (**2**) and the phenyl-sulfoquinoline advanced hit (**3**)

55
56
57
58
59 Our most important objective during the optimization of **3** was therefore to improve the metabolic
60 stability while maintaining target potency of phenyl-sulfoquinolines. Optimization of GPCR allosteric

1
2
3 modulators is a complex task due to multiple reasons.⁸ Structure-activity relationship of allosteric
4
5 modulators is commonly steep or flat,¹⁸ structural modifications might result in the switch between
6
7 NAMs and PAMs¹⁹ and the properties of allosteric sites often challenge the ADME properties of the
8
9 ligands. The latter situation frequently occurs when structural changes at metabolically vulnerable
10
11 moieties and attempts to improve the solubility are less tolerated by the SAR. In such cases iterative,
12
13 multidimensional parallel synthesis approaches^{20,21} might help to understand structure-activity and
14
15 structure-metabolism relationships. We herein report the successful implementation of this strategy
16
17 for the optimization of our phenyl-sulfoquinoline-based mGluR5 NAMs to clinical candidate **25**, and
18
19 preclinical data that support its potential in psychiatry indications.
20
21
22
23
24
25

26 Chemistry

27
28 4-Phenyl-3-aryl-sulfoquinolines were synthesized in five steps from substituted sodium arylsulfonates
29
30 (**4**). The arylsulfonates were first converted to methyl 2-(arylsulfonyl)acetates (**5**) with
31
32 ethylchloroacetate in DMF. The reaction of arylsulfonyl acetates (**5**) and triethyl orthoformate gave
33
34 methyl 3-ethoxy-2-(arylsulfonyl)-2-propenoates (**6**) that were cyclized to corresponding quinolinones
35
36 (**8**) with substituted anilines (**7**). Phenylsulfonyl-4(1H)-quinolinones (**8**) were chlorinated by POCl₃ in
37
38 position 4 preparing the corresponding 4-chloro-3-phenylsulfonyl-quinolines (**9**) that were coupled
39
40 with boronic acids (**10**) in 1,4-dioxane using Pd(PPh₃)₄ and K₂CO₃ to give 4-phenyl-3-aryl-
41
42 sulfoquinolines (**11**) (Scheme 1).
43
44
45
46
47
48
49
50
51
52
53
54
55
56
57
58
59
60



Scheme 1. Synthesis of 4-phenyl-3-aryl-sulfoquinolines

i – DMF, $\text{ClCH}_2\text{COOEt}$, 1 h at 80°C , 60-80%; ii – $\text{HC}(\text{OEt})_3$, 3 h at 150°C , 90-95%; iii – PhOPh , reflux 1 h, 35-55%; iv – POCl_3 , reflux 2-3 h, 90-95%; v – 1,4-dioxane, $\text{Pd}(\text{PPh}_3)_4$, K_2CO_3 , 20h at 90°C , 50-90%.

Results and Discussion

Our optimization strategy involved a multiple parallel synthesis approach as applied for all the three regions of 4-phenyl-3-aryl-sulfoquinolines (Figure 3).

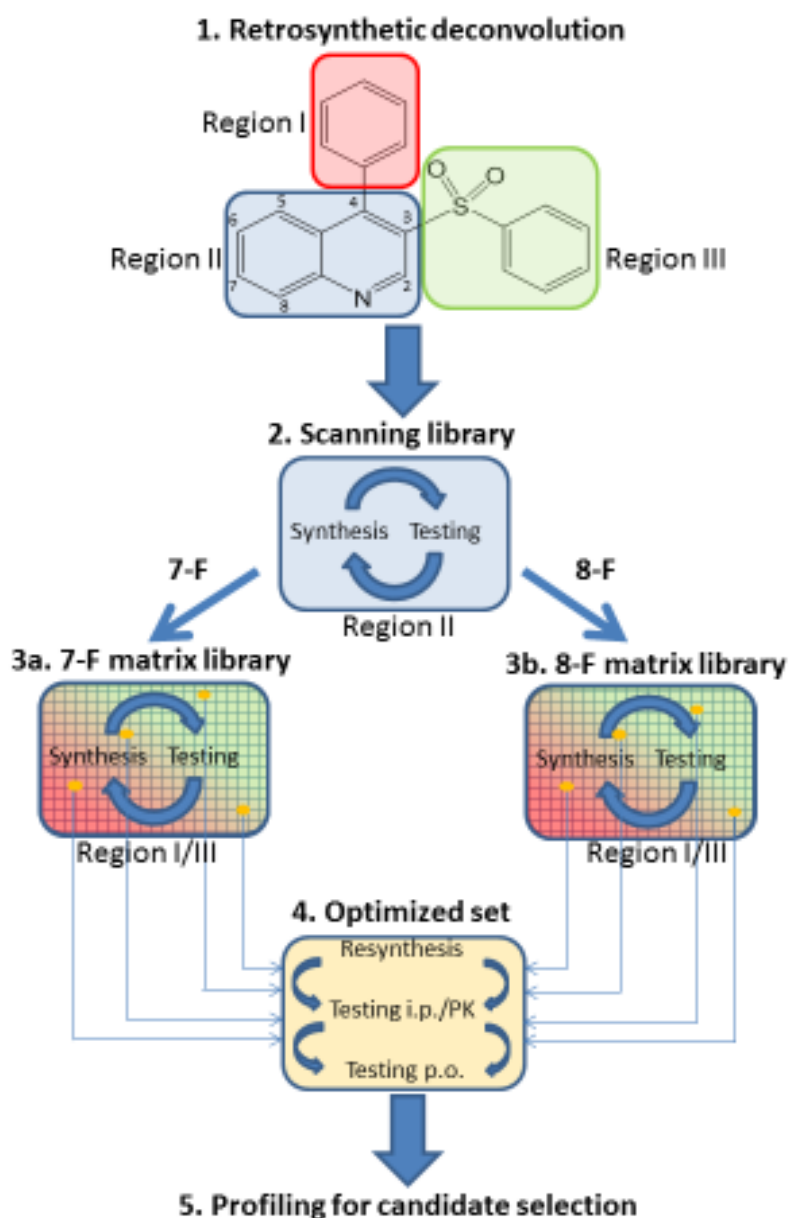
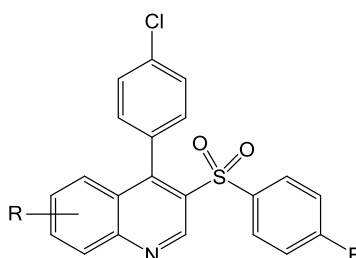


Figure 3. Implementation of the multiple parallel synthesis approach for the optimization mGluR5 NAMs. Retrosynthetic analysis of the sulfoquinoline scaffold at level 1 allowed us to identify three regions (Regions I, II and III) for further evaluation. The preferred substituents in Region II (7-fluoro and 8-fluoro) were identified by the scanning library at level 2. Next we explored Regions I and III by the synthesis of matrix libraries 3a and 3b. Most promising compounds identified from the matrix libraries were further optimized at level 4 to yield compounds profiled for candidate selection at level 5.

Since our primary objective was to improve the metabolic stability the first step was that we analyzed the metabolically vulnerable positions of **3** by SmartCyp.²² The most affected para-methyl group in Region III was replaced by a fluorine substituent and metabolic hot spots of the modified core were re-evaluated. Since SmartCyp suggested all of the metabolic hot spots in Region II (see Supplementary Figure 1). The available positions of the quinoline core were mapped by the scanning library (Figure 3, Table 1).

Table 1. The effect of quinoline substituents on the binding affinity and metabolic stability of 4-phenyl-3-aryl-sulfoquinolines prepared in the scanning library



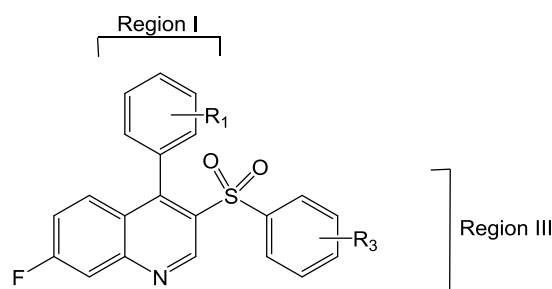
Compound	R	rat mGlu5 MMPEP displ. at 1 uM (%) ^a	rat mGlu5 binding K _i (nM) ^a	rat CL int (ml/min* ^a g liver) ^a	human CL int (ml/min* ^a g liver) ^a
12	6-Cl,7-F	43.7	n.d.	0.34	0.01
13	6-F,7-Cl	48	n.d.	0.57	0.01
14	7-Cl, 8-F	83.6	71.2	0.01	0.01
15	8-F	91.5	16	0.06	0.28
16	6-F	76.3	179.6	0.40	0.12
17	7-F	91.6	38.6	0.89	1.23
18	6-Cl	58.3	n.d.	0.20	0.01
19	6-CN	39.7	n.d.	0.04	0.01
20	7-Cl	92.8	110.4	0.01	0.21
21	7-CN	8.7	n.d.	0.01	0.01
22	6-Cl, 8-F	19	n.d.	0.09	0.01

^a geometric mean, n ≥ 2 measurements

Scanning around the quinoline core revealed that the measured metabolic stabilities were in line with the SmartCyp predictions. The introduction of halogens to positions 6, 7 and 8 of Region II improves the metabolic stability in both species significantly. Similar to optimization programs reported against other allosteric GPCR sites we found the “fluorine walk” useful to identify the most

tolerant positions of the core.²³ In the case of 7- and 8-fluoro derivatives the improved metabolic stability went parallel to reasonable binding affinity towards the target. After we identified the optimal positions for fluorine incorporation we aimed to find the best combination of Region I and Region III substituents in terms of potency and metabolic stability. Consequently, at the next stage of our optimization protocol we used matrix libraries (3a and 3b on Figure 3) to understand structure-metabolism relationships around the 7- and 8-fluoroquinoline cores. During these attempts we mapped Regions I and III synthesizing two matrix libraries of 61 and 53 7-fluoro and 8-fluoro-sulfoquinolines, respectively by parallel synthesis (Scheme 1). Library members were first evaluated in metabolic stability assays using rat and human microsomes and also tested against mGluR5. Since human metabolic stability data ran parallel to corresponding rat data we restrict our analysis to human data (Figure 4).

A. Matrix library of 7-fluoroquinoline derivatives

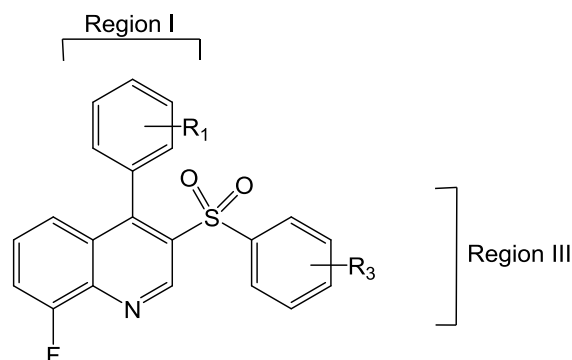


Intrinsic clearance, human (ml/min*g liver)

Region III

Region I	Region III												
	3-F	4-F	3-CN	3-OMe	4-OMe	3,4-Me2	3,4-F2	3,5-Cl2	3,5-F2	3-Cl,4-F	3-Cl,4-OMe	3-F,4-Me	average
2-F			1.39				0.79	0.93		1.07			1.05
3-F	0.24	0.95	0.78	3.36	2.94	3.71	0.60	0.41	0.06	0.25	2.08	0.41	1.32
4-F	0.11	1.34	0.39	9.37	1.71	9.25	0.44	0.18	0.01	0.69	1.29	2.33	2.26
3-Cl			0.99	2.97		4.01	0.38	0.93	0.22	0.66	1.19	2.13	1.50
4-Cl	0.98	1.25	0.31		1.28	7.88	0.01	0.13	0.03	0.39			1.36
3-OMe			1.83			8.78	1.77	1.51	1.81		1.71		2.90
4-OMe	1.89	1.77	0.92		1.18	4.13	1.10	1.00	1.51	1.08			1.62
average	0.81	1.33	0.94	5.23	1.78	6.29	0.73	0.73	0.61	0.69	1.57	1.62	

B. 8-fluoroquinoline derivatives



Intrinsic clearance, human (ml/min*g liver)

Region III

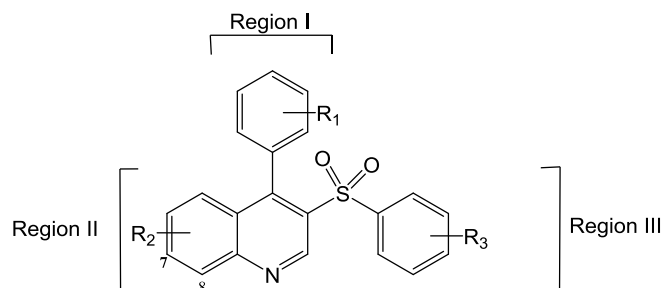
	3-F	4-F	3-CN	4-OMe	3,4-F2	3,5-Cl2	3,5-F2	3-Cl,4-F	3-F,4-Me	average
2-F	0.21		0.66		1.39	0.44	0.09	1.39		0.70
3-F	1.14	1.56	0.34	3.03	1.28	1.08	1.18	1.23	3.92	1.64
4-F	0.19		0.19		0.78	1.01	0.69	0.19	2.75	0.83
3-Cl	0.56	1.21	1.11	2.75	1.13	1.20	0.64	0.18	3.18	1.33
4-Cl	0.62	0.28	0.08	1.05	0.28	0.78	0.73	0.01	2.20	0.67
3-OMe	2.60	2.23		2.87		2.31	2.76		4.02	2.80
4-OMe	2.48	2.41		2.12	2.12	2.11	2.59		3.27	2.44
average	1.11	1.54	0.48	2.36	1.16	1.27	1.24	0.60	3.22	

Figure 4. Metabolic stability driven optimization of Region I and III substituents around the sulfoquinoline core. Panel A shows human intrinsic clearance data in the 7-fluoroquinoline library (matrix library 3a). The library contains 61 derivatives carrying a range of substituents in Region I (rows) and Region III (columns). Panel B shows human intrinsic clearance data in the 8-fluoroquinoline library (matrix library 3b). The library contains 53 derivatives carrying a range of substituents in Region I (rows) and Region III (columns). Cells are colored as a gradient from red (high clearance) to green (low clearance).

1
2
3 Analyzing the impact of the 7-fluoroquinoline substituents we concluded that 4-chloro, 4-fluoro and
4
5 3-fluoro substituents were beneficial in Region I, while methoxy groups introduced to positions 3 and
6
7 4 resulted in much less stable compounds. Although 4-chloro derivatives were somewhat better than
8
9 4-fluoro compounds this trend was reversed at position 3, showing 3-chloro derivatives as less stable
10
11 compounds as their corresponding fluoro analogues. Region III generally preferred disubstituted
12
13 analogues since difluoro, dichloro and mixed fluoro-chloro compounds showed better metabolic
14
15 stability as compared to mono-substituted compounds. The only exceptions were 3-fluoro and 3-
16
17 cyano substituents that gave similar metabolic stability as the disubstituted analogues. Position 3
18
19 seems to be crucial in this region since stable disubstituted analogues always contain a fluorine or
20
21 chlorine atom in this position. Otherwise 3,4- and 3,5-disubstitutions gave similar results. In contrast
22
23 to halogen substituents both methoxy and methyl derivatives were found to be metabolically less
24
25 stable in mono- and disubstituted scenarios, respectively. Structure-metabolism relationship was
26
27 found to be similar for 8-fluoroquinolines as both 4-chloro and 4-fluoro substituents were beneficial
28
29 in Region I. Methoxy substituents in positions 3 and 4 yielded significantly less stable compounds. 2-
30
31 fluoro derivatives were metabolically more stable and the 3-fluoro substituent seems to be less
32
33 favored than found in the 7-fluoroquinoline series. Preferred substituent patterns of Region III
34
35 showed high similarity to that observed for 7-fluoroquinolines. Again, 3-fluoro and 3-cyano
36
37 derivatives emerged from the mono-substituted analogues, while 3,4- and 3,5-dihalo substitution
38
39 gave compounds with acceptable metabolic stability. Methyl and methoxy substituents mostly
40
41 increased the metabolic vulnerability of 8-fluoroquinolines.

42
43
44 Combining the results of this structure-metabolism analysis with the binding affinity data we selected
45
46 the most stable and mGluR5 active ($K_i < 50$ nM) library members and resynthesized them for *in vivo*
47
48 testing (Figure 3). The optimized set of 4-phenyl-3-aryl-sulfoquinolines was evaluated in the Vogel
49
50 punished drinking test after i.p. administration. Compounds showed reasonable MED (lower than 30
51
52 mg/kg) were also tested after p.o. administration (Table 2).
53
54
55
56
57
58
59
60

Table 2. Best 4-phenyl-3-aryl-sulfoquinolines identified from the matrix libraries.



Cmpd	R ₁	R ₂	R ₃	rat mGluR5 binding K _i (nM) ^a	human mGluR5 functional IC ₅₀ (nM) ^a	rat CL (ml/min* g liver) ^a	human CL (ml/min* g liver) ^a	Vogel i.p. MED (mg/kg)	Plasma level at Vogel MED ^b (nM)	Vogel p.o. MED (mg/kg)	Plasma level at Vogel MED ^c (nM)
MPEP ²⁴	-	-	-	9.6	31	0.19	1.61	3	n.d.	3	n.d.
23	4-F	7-F	3-Cl, 4-F	5.2	21	0.89	0.69	10 ^e	71.0	3 ^f	133
24	4-F	7-F	3-CN	6.5	20	0.70	0.39	10 ^e	208	10 ^e	88.3
25	4-F	7-F	3-CN	6.5	20	0.70	0.39	10 ^e	208	3 ^f	151
26	4-Cl	7-F	3-CN	55.3	133	0.25	0.31	3 ^e	51.1	0.5 ^f	34.8
27	3-F	7-F	3,5-Cl ₂	10.7	35	1.53	0.41	30 ^e	90.6	n.t.	n.d.
28	4-F	7-F	3,5-F ₂	18	25	0.93	0.01	>30 ^e	206 ^d	>10 ^f	n.d.
29	4-F	8-F	3,5-Cl ₂	6.8	25	1.06	1.01	30 ^e	119	n.t.	n.d.
30	4-F	8-F	3-F	31.6	69	0.20	0.19	30 ^e	1207	n.t.	n.d.
31	4-F	7-F	3,5-Cl ₂	11.5	25	1.15	0.18	>30 ^e	165 ^c	n.t.	n.d.
32	3-F	7-F	3,5-F ₂	32.6	74	1.80	0.06	>30 ^e	63.0 ^d	n.t.	n.d.
33	4-F	7-F	3,4-F ₂	19.1	43	0.67	0.44	>30 ^e	247 ^d	n.t.	n.d.
34	4-Cl	7-F	3-Cl, 4-F	8.3	27	0.45	0.39	30 ^e	373	10 ^e	373
35	4-Cl	7-F	3-Cl, 4-F	8.3	27	0.45	0.39	30 ^e	373	3 ^e	218
36	4-F	8-F	3,5-F ₂	13.3	12	0.63	0.69	30 ^e	151	n.t.	n.d.
37	4-Cl	7-F	3,5-Cl ₂	30.3	94	0.77	0.13	30 ^e	377	n.t.	n.d.
38	4-Cl	8-F	3,4-F ₂	8.4	13	0.20	0.28	3 ^e	59.7	>30 ^e	196 ^d
39	4-Cl	7-F	3,4-F ₂	17.1	22	1.41	0.01	10 ^e	n.d.	10 ^e	n.d.

n.t. – not tested, n.d. – not determined, ^a geometric mean, n ≥ 2 measurements, ^b ~45 minutes after ip. administration, ^c ~75 minutes after p.o.

administration, ^d at the dose of 30 mg/kg, ^e in suspension containing 5% Tween 80, ^f in Type IV lipid formulation diluted with 70% d.w stabilized with 1% HPMC

Based on *in vivo* evaluation we found five compounds that showed high anxiolytic efficacy in both i.p. and p.o. administration. Since most of the present anxiolytics show memory impairment as a dose limiting side effect we tested four compounds out of the five in the Morris water maze at a single dose of 30 mg/kg (Table 3).

Table 3. Effect of selected 4-phenyl-3-aryl-sulfoquinolines on learning performance as evaluated in the Morris water maze test.

Compound	Test dose (mg/kg)	Outcome	Plasma level (nM)	Therapeutic index (Morris MED/Vogel MED)	Therapeutic index (plasma levels)
23	30 ^a	Slight impairment	968	≤10	≤9.1
24	30 ^a	Impairment	1280	10	≤8.4
25	30 ^a	No impairment	986	>30	28.3
33	30 ^b	Slight impairment	866	10	3.9

^a Type IV lipid formulation diluted with 70% d.w stabilized with 1% HPMC, ^b Type IIB lipid formulation diluted with 70% d.w

Interestingly we found, that except for compound **25** all the other compounds affected the learning performance showing slight to moderate impairment at 30 mg/kg. Clinical signs together with therapeutic indices calculated from both MED values and plasma levels obtained in the main effect and the side effect animal models suggested compound **25** as the ultimate choice. The compound was therefore nominated as a development candidate selected for further characterization.

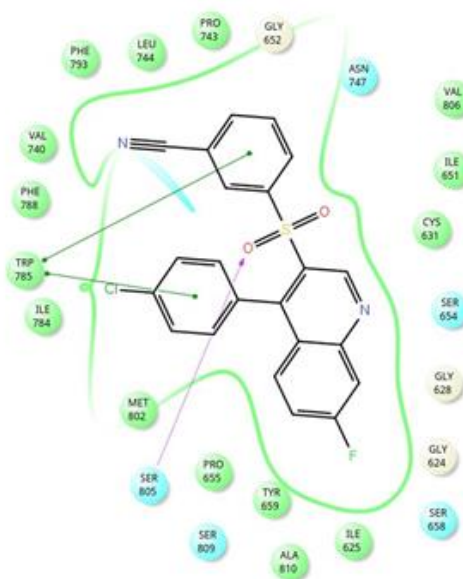
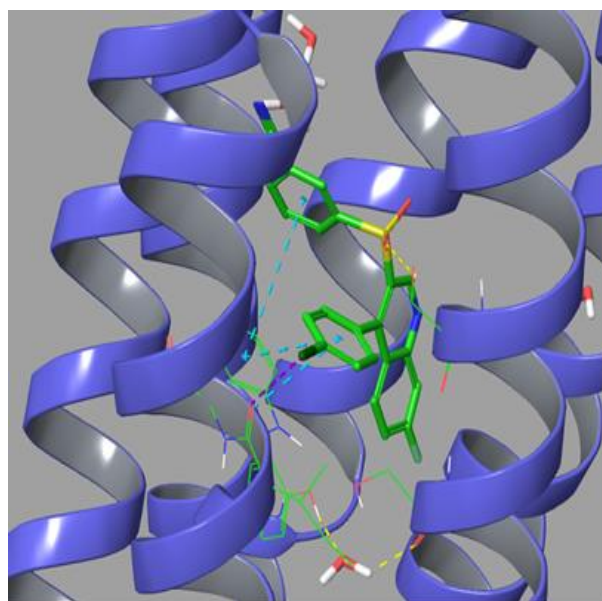
Characterization of compound **25**

Binding mode to mGluR5

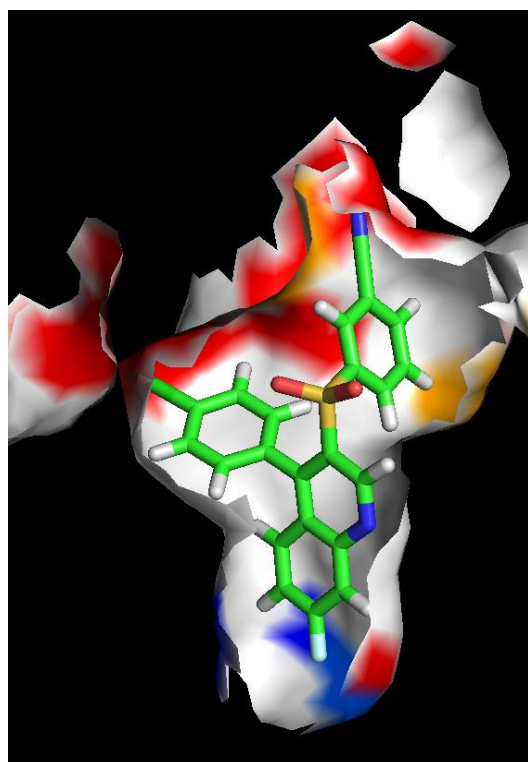
The first step of the characterization of the development candidate involved the investigation of key interactions formed in the binding site of mGluR5 (Figure 5). Since 4-phenyl-3-aryl-sulfoquinolines differ significantly from earlier acetylenic mGluR5 NAMs we used the the high resolution X-ray structure of compound **1** a non-acetylenic chemotype cocrystallized with mGluR5.¹⁴ Docking calculations revealed that similar to compound **1** the sulfoquinoline core and the fluorine substituent in Region II is located in a pocket formed by Pro655^{3,40}, Tyr659, Ala810^{7,40}, Ile625^{2,46}, Ser658^{3,43}, Gly624, Gly628^{2,49} and Ser654^{3,39} (Ballesteros-Weinstein²⁵ numbering in superscript). Direct comparison of binding modes, however, showed that the extended conformation of **25** prevents its binding in the lower part of the pocket occupied by **1**. As a consequence, unlike to the Heptares compound the quinolone nitrogen of compound **25** could not form hydrogen bond to Ser809^{7,39}. Instead, the expected

1
2
3 binding mode suggests that one of the sulfone oxygens of **25** makes a hydrogen bond with Ser805^{7.35}
4
5 opposite to Ser809^{7.39}. One of the most significant differences between the conformations of binding
6
7 site residues around **1** and mavoglurant is related to Trp785^{6.50}. In the case of **1** this residue is rotated
8
9 out toward helix 5 and forms aromatic interactions with the ligand. Interactions with Trp785^{6.50} were
10
11 also crucial for our compound since the phenyl rings of both Regions I and III were found in aromatic
12
13 stacking with this residue. Compound **1** formed similar interactions with Phe788^{6.53} but this residue
14
15 seems to be less relevant in the binding of **25**. The orientation of the 3-aryl substituent of the
16
17 sulfoquinoline core (Region III) is similar to that of the 3-chloro-5-cyanophenyl ring of **1** this allows
18
19 formation of a water mediated hydrogen bond between the 3-cyano substituent in Region III with the
20
21 backbone carbonyl of Val740^{5.40}.
22
23
24
25
26
27
28
29
30
31
32
33
34
35
36
37
38
39
40
41
42
43
44
45
46
47
48
49
50
51
52
53
54
55
56
57
58
59
60

A.



B.



C.

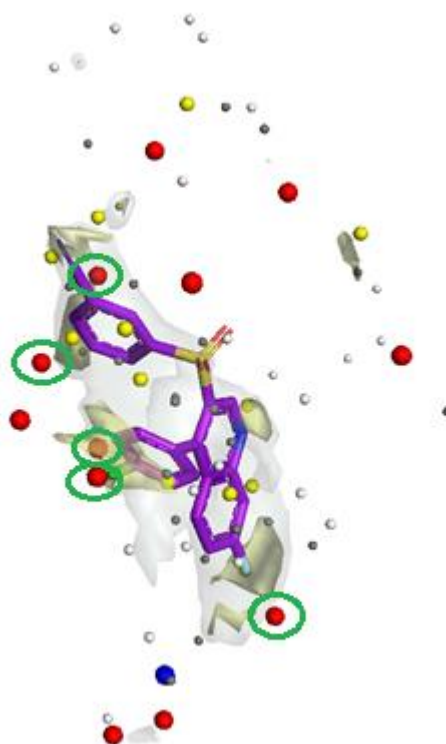


Figure 5. The predicted binding mode of **25** (A), binding hot spot map (B) and lipophilic hot spots (C) of its binding site. The color coding of the binding hot spot map (B) reflects the GE of all ligands described in Table 3 and is projected on the protein atoms within 4 Å distance. The binding pocket surface was

1
2
3 colored according to the maximum GE values for each protein atom. Oxygen, nitrogen, sulphur and
4
5 hydrogen atoms are colored red, blue, orange and white, respectively. Lipophilic hot spots (yellow
6
7 shaded surfaces on panel C) were identified by WaterFLAP²⁶ at the binding site found in the X-ray
8
9 structure of mGluR5-compound **1** complex without the ligand (gray surface). Waters are color coded
10
11 to show the energetically most disfavored as red (>3.5 kcal/ mol), then yellow (2.2–3.5 kcal/mol), bulk
12
13 solvent as gray (–1 to 2.2 kcal/mol), and favored as blue (<–1 kcal/mol). GRID maps are contoured
14
15 (transparent solid) and colored in the following manner: CH₃ methyl group probe in gray at 1 kcal/mol
16
17 defining the pocket surface and C1= probe (lipophilic) in yellow at –2.7 kcal/ mol. The predicted binding
18
19 mode of **25** (purple) is overlaid to identify the displaced water molecules (green circled).
20
21
22
23
24

25
26 The predicted binding mode of **25** was validated by the hot spot analysis of the binding site using
27
28 structure–activity relationship (SAR) data available in Table 1 and 2. We used the group efficiency (GE)
29
30 concept²⁷ to analyze the contributions of different parts of the ligand to its binding affinity. All ligands
31
32 with measured K_i values (Tables 1 and 2) were docked to the binding site identified for **25**, the best
33
34 scored pose was selected and the GEs of all ligands were projected on the protein surface resulting in
35
36 different hot spots. Hot spot analysis (Figure 5 B) revealed that Region II substituents around the lower
37
38 part of the quinoline ring (positions 7 and 8) contribute most significantly to the binding affinity and
39
40 therefore identified as primary hotspot. The secondary hot spot is located around the benzenesulfonyl
41
42 ring (Region III) represented by positions 3 and 5. Finally, the phenyl ring at position 4 of the quinoline
43
44 core (Region I) fits well to the nearby lipophilic hot spot (Figure 5 C). WaterFLAP calculations showed
45
46 that the binding of **25** involves the displacement of water molecules in all regions. In Region II the 7-
47
48 chloro substituent of **25** reaches the lipophilic hot spot at the bottom of the binding site and more
49
50 importantly displaces the water molecule critical for receptor activation.²⁸ Substituents at positions 3
51
52 and 4 around the 4-phenyl ring (in Region I) also displace energetically disfavored water molecules.
53
54 Finally, substituents at positions 3 and 5 around the upper phenyl group in Region III displace the
55
56 corresponding disfavored waters while the nitrile substituent forms a bridged H-bond to Val740^{5,40}.
57
58
59
60

1
2
3
4
5
6
7
8
9
10
11
12
13
14
15
16
17
18
19
20
21
22
23
24
25
26
27
28
29
30
31
32
33
34
35
36
37
38
39
40
41
42
43
44
45
46
47
48
49
50
51
52
53
54
55
56
57
58
59
60

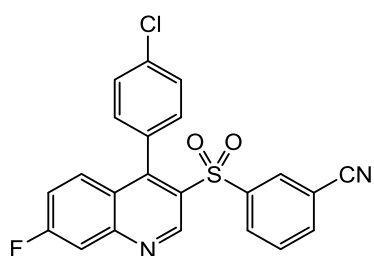
Primary in vitro pharmacology and in vitro ADME

Compound **25** is a potent and selective negative allosteric modulator at mGluR5 metabotropic glutamate receptors (Table 4). Its potency on mGluR5 was assessed in comparison to mGluR1 in various assays including recombinant human and native rat and human receptors. Moreover, functional activity of the compound was characterized on recombinant human and native rat mGluR5 and native rat mGluR1. [³H]-M-MPEP radioligand displacement studies²⁹ were done using three types of membranes prepared from (i) rat cerebrocortical tissue (ii) human mGluR5 expressing recombinant cell line and (iii) post mortem human parietal cortical tissue. Selectivity of **25** to mGluR5 vs. mGluR1 was investigated in [³H]-R214127 binding assays³⁰ with membranes prepared from (i) rat cerebellar tissue (ii) human mGluR1 expressing recombinant cell line and (iii) post mortem human cerebellar tissue. In conclusion, compound **25** binds with high affinity to the allosteric binding site of native (rat and human) as well as recombinant (human) mGluR5 receptors and exhibits a selectivity of >50-fold over native mGluR1 receptors. Functional studies in cells expressing mGluR5 or mGluR1 receptors were performed by fluorometric calcium measurements with the group I specific agonist DHPG ((S)-3,5-dihydroxyphenylglycine) in CHO cells expressing recombinant human mGluR5a receptors (hmGluR5-CHO; EuroScreen), primary neuronal cultures prepared from neocortices of E17 rat embryos (expressing predominantly mGluR5), and also from cerebelli of newborn rat pups (expressing predominantly mGluR1). In conclusion, compound **25** behaves as a functional antagonist at both mGluR5 and mGluR1 receptors with considerable selectivity for mGluR5 receptors. Broad selectivity profiling against 68 receptors, ion channels at the test concentration of 1 μM revealed no significant activity (<30 % effect) at any of the targets.

Penetration of compound **25** through MDCKII-MDR1 cell monolayers, a surrogate *in vitro* model of brain penetrability, was measured for both inward and outward directions. The calculated apparent inward permeability (*P_{app}*) value and permeability directional ratio (PDR, i.e. *P_{app}*_{outward}/*P_{app}*_{inward}) are both reasonable and show that the compound can penetrate through membranes and is not a

likely substrate of efflux transporters. The *in vitro* metabolism of compound **25** was investigated using rat, dog and human liver microsomes. The amount metabolized was the highest in monkey liver microsomes and similar among liver microsomes of human, mouse and rat. The potential of **24** to inhibit CYP1A2, CYP2C9, CYP2D6 and CYP3A4 enzymes was investigated using human liver microsomes and their specific probe substrate(s). The apparent IC₅₀ of compound **25** for the inhibition of the enzymes tested was higher than 10 μM, suggesting that **25** is not a potent inhibitor of these enzymes.

Table 4. Summary of *in vitro* pharmacology and ADME data for **25**



Property	Value	
Physicochemical		
MW	422.9	
logD (pH 7.4, calculated)	5.3	
tPSA	70.3	
aqueous solubility (μg/mL, pH 7.4, measured)	10	
mGluR5 binding (nM)		
Rat native mGluR5 K _i	5.3	
Human recombinant mGluR5 K _i	4.9	
Post mortem human mGluR5 K _i	Male	10.8
	Female	12.1
mGluR5 functional activity (nM)		
Human recombinant mGluR5 IC ₅₀	13	
Rat native mGluR5 IC ₅₀	19	
Papp (nm/s) inward	115	
PDR	0.74	
Intrinsic clearance, (ml/min*g liver)	Rat	0.25
	Dog	0.27
Plasma protein binding, (bound (%))	Human	0.31
	Rat	99.73
	Dog	99.75
	Human	99.61

Preclinical disposition

Detailed pharmacokinetic (PK) investigations were performed after single dose i.v. and oral administration of **25** to Crl:CD(SD) rats and beagle dogs and a pilot single dose PK study was conducted in Cynomolgus monkeys with oral (nasogastric) administration in different lipid based formulations.³¹ Disposition properties of the compound were also investigated in rats after *per os* administration of ¹⁴C-labelled compound **25** ([¹⁴C]-**25**). Table 5 shows the PK parameters for the unchanged compound **25** and summarizes the PK parameters for the total radioactivity (compound unchanged + metabolites) after the administration of its ¹⁴C-labelled form.

Table 5. Mean pharmacokinetic parameters for **25**

Species	Sex (No. of animals)	Route	Formulation	Dose mg/kg	Cl mL/h/kg	V _d L/kg	t _{1/2} h	T _{max} h	C _{max} nM	⁺ AUC _{tot} nM.h
Rat Crl:CD(SD)	M (n=3)	iv.	80% cosolvent mixture/20% d.w.	0.5	1674	12.4	5.13	--	--	707
	F (n=3)				856	9.6	7.79			1381
	M (n=3)	p.o. fed	undiluted Type IV lipid formulation	4.5	--	--	7.06	0.75	369	2190
	F (n=3)						6.30	0.75	650	7297
Dog Beagle	M (n=3)	iv. inf.	80% cosolvent mixture/20% d.w.	0.5	386	8.6	12.2	0.5	1542	3074
	F (n=3)				553	9.2	11.8	0.5	1144	2218
	M (n=3)	p.o. *fasted	undiluted Type IV lipid formulation	1	--	--	12.8	0.75	492	1859
	F (n=3)						10.7	0.83	551	1684
Cynom. monkey	M (n=3)	p.o. &fasted	undiluted Type IV lipid formulation	9	--	--	1.4 [#]	1.7 [#]	57 [#]	132 [#]
	F (n=3)						2.1 [#]	1.3 [#]	33 [#]	87 [#]

[#] median, * from 1h prior to dose until 2h post dose, [&] from 2h prior to dose until 2h post dose ⁺AUC₀₋₈ in monkey study

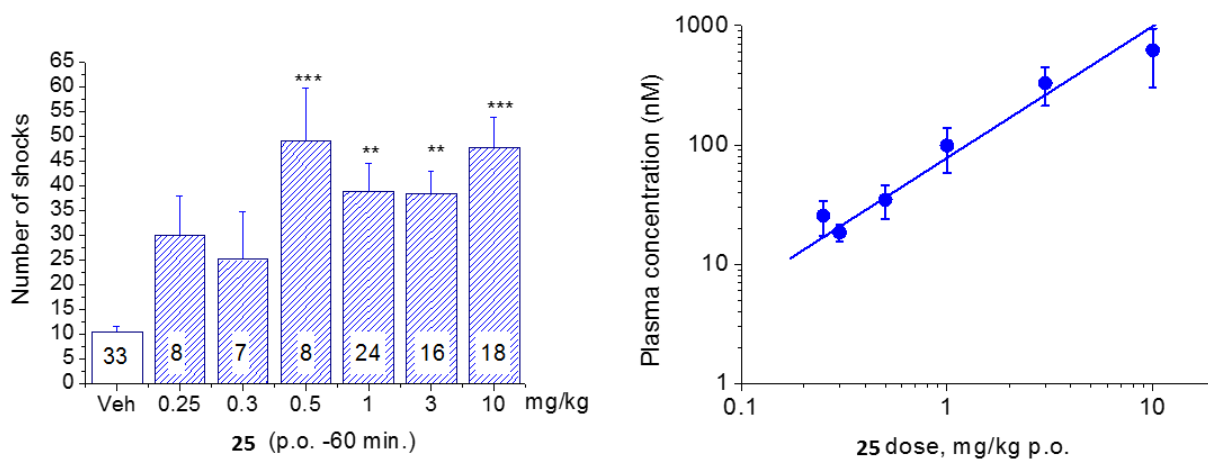
Our results showed that the distribution volume was very similar in the rat and the dog (9-12 L/kg), but with higher clearance in rat over dog (856-1674 mL/h/kg for the rat and 386-553 mL/h/kg for the dog), resulting in lower half-life values (5-8 h) in the rat compared to dog (~12 h). The t_{1/2} of compound **25** in monkeys was even shorter (1-2 h), indicating substantially higher systemic clearance in this

1
2
3 species. The pharmacokinetic parameters were similar between the genders, although female rats
4
5 seemed to show somewhat lower clearance than male rats. In contrast, female dog had higher
6
7 clearance than the male. These findings are in accordance with the *in vitro* metabolic stability data,
8
9 which show highest rate of metabolism in monkey liver microsomes followed by rat and human. The
10
11 terminal elimination half-life in the rat was similar for the unchanged **25** (~7 h after oral 4.5 mg/kg)
12
13 and the total [¹⁴C]-**25** related radioactivity (~8 h after oral 50 mg/kg), suggesting that that there was
14
15 no long-persisting major metabolite.
16
17
18
19
20

21 ***In vivo* pharmacology**

22
23
24 *Anxiolytic efficacy* - Investigation of compound **25** in the Vogel punished drinking test was accompanied
25
26 with plasma level determinations from the same animals right after the test. The compound was
27
28 administered as a single dose in different lipid based formulations.³¹ Dose–response relationship of **25**
29
30 was determined in four separate experiments; the pooled results are shown in Figure 6.
31
32
33
34
35
36
37
38
39
40
41
42
43
44
45
46
47
48
49
50
51
52
53
54
55
56
57
58
59
60

A.



B.

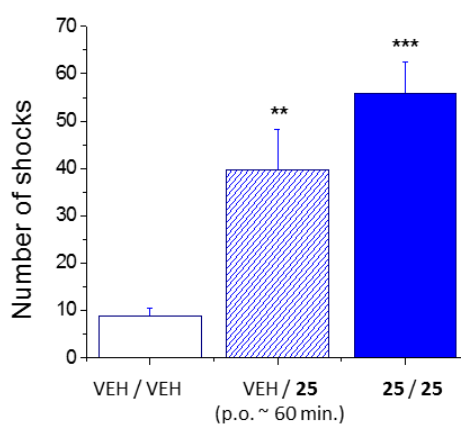


Figure 6. Anxiolytic efficacy of **25** in the Vogel punished drinking test after single and repeated dose p.o. administration. A. Anxiolytic effect of single doses of **25** in the Vogel assay (A) and plasma levels measured right after the test (B). Mean±SEM values are given in (A), group sizes are shown inside the columns. *, ** and ***: $p < 0.05$, $p < 0.01$ and $p < 0.001$, respectively, vs. vehicle-treated group (ANOVA followed by post-hoc Duncan-test). In (B), mean±SD values are plotted. B. Effect of repeatedly administered **25** in the Vogel test. Means±SEM values are shown. Group size was 10. VEH/VEH: vehicle-treated control group, VEH/**25**: single dose compound **25** treated group, **25**/**25**: repeat dose compound **25** treated group. ** and ***: $p < 0.01$ and $p < 0.001$, respectively, vs. VEH/VEH. (ANOVA followed by post-hoc Duncan-test).

1
2
3 Compound **25** was active in the Vogel punished drinking test with a minimum effective dose of 0.5
4 mg/kg, with apparently dose-independent efficacy (ceiling effect) in the range of the 0.5-10 mg/kg.
5
6
7 Plasma concentrations of **25** increased approximately proportionally with increasing doses. For
8 assessment of plasma concentrations associated with maximum efficacy, doses of 0.5 and 1 mg/kg
9
10 yielded mean plasma concentrations of 34.8 nM and 99 nM, respectively. Impact of repeated
11
12 administration on the anxiolytic effect of **25** was investigated in the Vogel assay. The compound was
13
14 administered once a day for 19 days at the dose of 10 mg/kg p.o. A vehicle-treated group which only
15
16 received drug injection on Day 19 served as the first-dose-effect control group. Compound **25**
17
18 produced statistically significant anxiolytic effects both after the first dosing and following 19-day-long
19
20 repeat-dose administration (0). Although plasma level of the compound was lower after repeated
21
22 dosing than after single dosing (513 ± 127 nM vs. 787 ± 323 nM; mean \pm SD), the anxiolytic efficacy rather
23
24 tended to increase indicating lack of development of tolerance to the anxiolytic effect of **25** at a
25
26 relatively high dose level.
27
28
29
30
31
32

33 The anxiolytic efficacy of **25** has been further demonstrated in ultrasonic vocalization test and
34 contextual fear-conditioning test. Compound **25** applied in the dose-range of 0.3–10 mg/kg p.o.
35 significantly and dose-dependently reduced ultrasonic vocalization with an ED₅₀ value of 1.5 mg/kg. In
36
37 the contextual fearing test compound **25** in the dose-range of 0.5–3 mg/kg p.o. significantly and dose-
38
39 dependently reduced the freezing behavior with an ED₅₀ value of 0.95 mg/kg. In conclusion, **25** shows
40
41 consistent *in vivo* efficacy at low doses (0.5-2 mg/kg, p.o.) in three rat models of anxiolytic activity.
42
43
44
45
46
47
48

49 *CNS side effect profiling* - The effect of **25** on spatial learning performance was investigated in the
50 Morris water maze paradigm at an oral dose of 30 mg/kg given 1 hour prior to the first daily trial.
51
52 Compound **25** did not affect the learning performance of rats. Plasma level of the compound measured
53
54 right after the last trial on Day 4 was 986 nM, which is about 30-fold higher than the reference
55
56 therapeutic plasma concentration in the Vogel assay (Table 3) assuring a considerably high therapeutic
57
58 index.
59
60

The effect of **25** (0, 10, 30 and 50 mg/kg, p.o.) on spontaneous locomotor activity was tested in male Wistar rats in a photocell-based activity monitor. Compound **25** dose-dependently inhibited locomotion with about 50% inhibition at 50 mg/kg p.o. dose. The lower doses did not significantly affect the ambulatory movement of rats. Therefore, the no observed adverse effect level in the study was 30 mg/kg.

Benchmarking 25 with diazepam - For benchmarking, we compared **25** to diazepam, the gold standard anxiolytic compound. Main effect and side effect profiles are shown in Table 6. The assay conditions for diazepam were the same as described above for compound **25**.

Table 6. Head-head comparison of **25** and diazepam in main and side effect pharmacology tests (doses are p.o. unless otherwise stated).

Effect	Test	25 dose mg/kg	25 plasma level nM	diazepam dose mg/kg	diazepam plasma level nM
Anxiolytic effect	Vogel test (MED)	0.5	34.8	2.5	BQL (<35)
	USV (ED ₅₀)	1.5	n.d.	7.8	n.d.
	Fear-conditioning (ED ₅₀)	0.95	n.d.	>10	n.d.
Side effects	Morris water-maze (MED)	>30	986	5 (i.p.)	n.d.
	SMA (ED ₅₀)	50	n.d.	9.7	n.d.

n.d. – not determined; MED: minimum effective dose; USV: ultrasonic vocalization; SMA: spontaneous motor activity

In general, **25** proved to be more potent than diazepam in the anxiolytic assays. Moreover, diazepam shows sedative and learning impairing effects at doses 1-4 fold higher than those of its anxiolytic-like activity. In contrast, **25** has about 30-fold therapeutic index between plasma levels associated with therapeutic (anxiolytic) and side effects.

Conclusion

Optimization of an amino-sulfoquinoline HTS hit led to identification of a 4-phenyl-3-arylsulfoquinoline lead. Extensive optimization around the sulfoquinoline core was supported by multiple parallel

1
2
3 syntheses of scanning and matrix libraries that provided highly potent mGluR5 NAM compounds with
4 enhanced metabolic stability. Further characterization of these library members resulted in the orally
5
6 bioavailable compound **25** which showed efficacy in a preclinical model of anxiety after both single a
7
8 repeated dose administration. Being a potent and selective mGluR5 NAM with acceptable ADME
9
10 properties, clean off-target profile, and favorable preclinical *in vivo* efficacy results, **25** was nominated
11
12 as clinical candidate and after profiling in regulatory toxicological studies was advanced to phase 1
13
14
15 clinical trials. Clinical data on human pharmacokinetics, safety and tolerability will be reported in due
16
17
18 course.
19
20
21
22
23
24
25

26 **Experimental Section**

27 *General Experimental Methods.*

28
29
30 All reactions were carried out under dry nitrogen. Commercially available reagents were used without
31
32 further purification. Solvents and gases were dried according to standard procedures. Organic solvents
33
34 were evaporated with reduced pressure using a rotary evaporator. Purity of final compounds was
35
36 assessed by HPLC with UV detection at 215 nm; all tested compounds were >95% purity. NMR spectra
37
38 were recorded on a Varian 500 MHz spectrometer equipped with a 1H{13C/15N} Triple Resonance 13C
39
40 Enhanced Salt Tolerant Cold Probe in DMSO-d6. Chemical shifts are referenced to TMS. HRMS analyses
41
42 were performed on a Finnigan MAT 95 XP mass spectrometer (Finnigan, Bremen, Germany). The
43
44 ionization method was EI and operated in positive ion mode. The ion source temperature was set at
45
46 220°C, the applied ionization energy was 70 eV. Data acquisition and analysis were accomplished with
47
48 Xcalibur software version 2.0 (Thermo Fisher Scientific Inc.). The quinoline part, the benzenesulfonyl
49
50 moiety, and the third ring of the molecules are numbered as <1...8a>, <1'...6'> and <1''...6'' or 7''
51
52 depending on the structure>, respectively. Melting points were determined in open glass capillaries
53
54 using Büchi 540 melting point apparatus and are uncorrected.
55
56
57
58
59
60

1
2
3 *General Procedure for the synthesis of 4-R3-aryl-R2-3-(R1- arylsulfonyl)-quinolines (Scheme 1)*
4

5 STEP1: The mixture of ethylchloroacetate and sodium arylsulfinate (**4**) in DMF (1 mL/mmol) was stirred
6 and heated at 80°C for 2 h. The solution was diluted with water (3 mL/mmol). The separated oil was
7 extracted with chloroform and washed with water. The organic phase was evaporated in vacuo to give
8 methyl 2-(arylsulfonyl)acetates (**5**) in 60-80% yield. STEP2: An equimolar mixture of arylsulfonyl
9 acetate (**5**) and triethyl orthoformate was stirred at 150 °C for 3 h with simultaneous distillation of
10 ethanol, and then evaporated to dryness. The crude methyl 3-ethoxy-2-(arylsulfonyl)-2-propenoates
11 (**6**) were obtained in 90–95% yield and were used in the next step without purification. STEP3: The
12 mixture of 25 mmol of methyl 3-ethoxy-2-(arylsulfonyl)-2-propenoate (**6**) and 25 mmol of the
13 corresponding aniline (**7**) in 20 ml of diphenyl ether was heated at near reflux for 1 h. After cooling the
14 precipitate was filtered, washed with ether and crystallized from an appropriate solvent to give R2-3-
15 (R1-arylsulfonyl)-4(1H)-quinolinone (**8**) in 35-55% yield. STEP4: 10 mmol of R2-3-(R1-arylsulfonyl)-
16 4(1H)-quinolinone (**8**) in 50 mmol of POCl₃ was refluxed for 2-3 h. Excess POCl₃ was evaporated in
17 vacuo. The residue was extracted with chloroform and washed with water. The organic phase was
18 evaporated in vacuo yielding R2-4-chloro-3-(R1-arylsulfonyl)-quinoline (**9**) in 90-95%. STEP5: 0.2 mmol
19 of the corresponding R2-4-chloro-3-(R1-arylsulfonyl)-quinoline (**9**) and 0.3 mmol of R₃C₆H₄B(OH)₂ (**10**)
20 in 2 ml of 1,4-dioxane were stirred for 20 h at 90°C with 1 mmol of K₂CO₃ and 0.01 mmol of Pd(PPh₃)₄.
21 After cooling, chloroform (10 mL) was added; the mixture was purified by chromatography on silica gel
22 and subsequent crystallization from methanol to give the final product as 4-R3-aryl-R2-3-(R1-
23 arylsulfonyl)-quinolines (**11**) in 50-90% yield. All 4-phenyl-3-aryl-sulfoquinolines reported were
24 prepared by the general procedure.
25
26
27
28
29
30
31
32
33
34
35
36
37
38
39
40
41
42
43
44
45
46
47
48
49
50

51
52
53
54 *4-(4-Chlorophenyl)-3-tosylquinoline hydrochloride (3):* 4-(4-chlorophenyl)-3-tosylquinoline (40 mg,
55 0.102 mmol) - prepared according to the general procedure - was dissolved in ethyl acetate (15 ml)
56 then HCl solution in ethyl acetate (c = 1.6 M, 0.14 ml, 0.224 mmol) was added dropwise to the solution.
57
58
59
60 The precipitated solid was filtered, washed with ethyl acetate, and dried under vacuum. Yield: 35 mg

1
2
3 (80%). Mp: 184-186 °C. ¹H NMR (500 MHz, DMSO-*d*₆) δ 9.61 (s, 1H), 8.16-8.25 (m, 1H), 7.98 (ddd, *J*=8.4,
4
5 6.9, 1.4 Hz, 1H), 7.60-7.69 (m, 1H), 7.41-7.52 (m, 2H), 7.31-7.37 (m, 2H), 7.23-7.30 (m, 3H), 6.96 - 7.07
6
7 (m, 2 H), 2.36 (s, 3H). EI-HRMS: calcd for C₂₂H₁₆O₂NCIS [M_{base}]⁺: 393.05848; found: 393.05831; delta= -
8
9 0.4 ppm. EI-MS m/z(rel int%): 393(100); 392(57); 400(8); 328(18); 294(8); 286(11); 254(14); 238(8);
10
11 226(14); 203(16); 176(18); 139(7); 36(2).

12
13
14
15 *6-Chloro-4-(4-chlorophenyl)-7-fluoro-3-((4-fluorophenyl)sulfonyl)quinoline (12)*: Mp: 172 °C. ¹H NMR
16
17 (500 MHz, DMSO-*d*₆) δ ppm 9.67 (s, 1 H) 8.29 (d, *J*=10.0 Hz, 1 H) 7.46 - 7.55 (m, 4 H) 7.36 (d, *J*=7.8 Hz,
18
19 1 H) 7.27 - 7.34 (m, 2 H) 7.02 - 7.09 (m, 2 H). EI-HRMS: calcd for C₂₁H₁₁O₂NCl₂F₂S [M]⁺: 448.98501;
20
21 found: 448.98395; delta= -2.4 ppm. EI-MS m/z(rel int%): 449(100); 448(58); 414(3); 384(10); 349(9);
22
23 306(14); 289(7); 278(11); 255(25); 228(9); 219(12); 193(6) 159(3); 143(5); 95(7).

24
25
26
27 *7-Chloro-4-(4-chlorophenyl)-6-fluoro-3-((4-fluorophenyl)sulfonyl)quinoline (13)*: Mp: 173 °C decomp.
28
29 ¹H NMR (500 MHz, DMSO-*d*₆) δ ppm 9.65 (s, 1 H) 8.57 (d, *J*=7.3 Hz, 1 H) 7.46 - 7.55 (m, 4 H) 7.27 -
30
31 7.35 (m, 1 H) 7.11 (d, *J*=10.0 Hz, 1 H) 6.98 - 7.06 (m, 2 H). EI-HRMS: calcd for C₂₁H₁₁O₂NCl₂F₂S [M]⁺:
32
33 448.98501; found: 448.98429; delta= -1.6 ppm. EI-MS m/z(rel int%): 449(100); 448(55); 384(12);
34
35 349(8); 306(16); 290(7); 278(12); 255(23); 228(9); 219(11); 193(5) 159(3); 143(6); 95(7).

36
37
38 *7-Chloro-4-(4-chlorophenyl)-8-fluoro-3-((4-fluorophenyl)sulfonyl)quinoline (14)*: Mp: 180 °C decomp.
39
40 ¹H NMR (500 MHz, DMSO-*d*₆) δ ppm 9.71 (s, 1 H) 7.78 (dd, *J*=9.3, 6.9 Hz, 1 H) 7.44 - 7.57 (m, 4 H) 7.27
41
42 - 7.35 (m, 1 H) 7.10 (dd, *J*=9.3, 1.4 Hz, 1 H) 6.97 - 7.07 (m, 2 H). EI-HRMS: calcd for C₂₁H₁₁O₂NCl₂F₂S [M]⁺:
43
44 448.98501; found: 448.98385; delta= -2.6 ppm. EI-MS m/z(rel int%): 449(100); 448(47); 384(10); 350(7);
45
46 306(15); 290(7); 278(12); 255(24); 228(6); 219(11); 193(5) 159(3); 143(5); 95(7).

47
48
49
50 *4-(4-Chlorophenyl)-8-fluoro-3-((4-fluorophenyl)sulfonyl)quinoline (15)*: Mp: 169-170 °C. ¹H NMR (500
51
52 MHz, DMSO-*d*₆) δ ppm 9.68 (s, 1 H) 7.85 (ddd, *J*=10.5, 7.8, 1.1 Hz, 1 H) 7.63 (td, *J*=8.2, 5.1 Hz, 1 H) 7.50
53
54 - 7.56 (m, 2 H) 7.44 - 7.50 (m, 2 H) 7.23 - 7.35 (m, 2 H) 7.09 (d, *J*=8.5 Hz, 1 H) 7.01 - 7.06 (m, 2 H). EI-
55
56 HRMS: calcd for C₂₁H₁₂O₂NClF₂S [M]⁺: 415.02398; found: 415.02359; delta= -1.0 ppm. EI-MS m/z(rel
57
58 int%): 415(100); 414(42); 350(13); 316(6); 272(10); 256(8); 255(10); 244(11); 221(18); 194(9); 143(3);
59
60 95(4).

1
2
3 4-(4-Chlorophenyl)-6-fluoro-3-((4-fluorophenyl)sulfonyl)quinoline (**16**): Mp: 142-143 °C. ¹H NMR (500
4 MHz, DMSO-*d*₆) δ ppm 9.62 (s, 1 H) 8.33 (dd, *J*=9.3, 5.4 Hz, 1 H) 7.94 (ddd, *J*=9.3, 8.1, 2.9 Hz, 1 H) 7.45
5 - 7.55 (m, 4 H) 7.25 - 7.35 (m, 2 H) 6.99 - 7.07 (m, 2 H) 6.89 (dd, *J*=9.8, 2.8 Hz, 1 H). EI-HRMS: calcd for
6 C₂₁H₁₂O₂NCIF₂S [M]⁺: 415.02398; found: 415.02328; delta= -1.7 ppm. EI-MS m/z(rel int%): 415(100);
7 414(51); 350(15); 316(7); 272(11); 256(8); 255(8); 244(12); 221(22); 194(13); 143(3); 95(4).
8
9

10 4-(4-Chlorophenyl)-7-fluoro-3-((4-fluorophenyl)sulfonyl)quinoline (**17**): Mp: 168-169 °C. ¹H NMR (500
11 MHz, DMSO-*d*₆) δ ppm 9.65 (s, 1 H) 8.02 (dd, *J*=9.9, 2.7 Hz, 1 H) 7.59 (ddd, *J*=9.4, 8.3, 2.6 Hz, 1 H) 7.45
12 - 7.54 (m, 4 H) 7.35 (dd, *J*=9.3, 6.0 Hz, 1 H) 7.25 - 7.33 (m, 2 H) 7.00 - 7.07 (m, 2 H). EI-HRMS: calcd for
13 C₂₁H₁₂O₂NCIF₂S [M]⁺: 415.02398; found: 415.02343; delta= -1.3 ppm. EI-MS m/z(rel int%): 415(100);
14 414(52); 350(15); 316(6); 272(16); 256(8); 255(7); 244(14); 221(20); 194(15); 143(3); 95(4).
15
16

17 6-Chloro-4-(4-chlorophenyl)-3-((4-fluorophenyl)sulfonyl)quinoline (**18**): Mp: 196-198 °C. ¹H NMR (500
18 MHz, DMSO-*d*₆) δ ppm 9.65 (s, 1 H) 8.26 (d, *J*=9.1 Hz, 1 H) 8.02 (dd, *J*=9.0, 2.4 Hz, 1 H) 7.47 - 7.55 (m, 4
19 H) 7.26 - 7.34 (m, 2 H) 7.18 (d, *J*=2.2 Hz, 1 H) 7.01 - 7.09 (m, 2 H). EI-HRMS: calcd for C₂₁H₁₂O₂NCl₂FS
20 [M]⁺: 430.99443; found: 430.99410; delta= -0.8 ppm. EI-MS m/z(rel.int.%): 431(100); 396(3); 366(10);
21 332(7); 288(9); 271(9); 260(10); 237(23); 210(10); 201(11); 175(6).
22
23

24 4-(4-Chlorophenyl)-3-((4-fluorophenyl)sulfonyl)quinoline-6-carbonitrile (**19**): Mp: 167-168 °C. ¹H NMR
25 (500 MHz, DMSO-*d*₆) δ ppm 9.77 (s, 1 H) 8.38 (d, *J*=8.6 Hz, 1 H) 8.29 (dd, *J*=8.7, 1.9 Hz, 1 H) 7.79 (d,
26 *J*=1.8 Hz, 1 H) 7.45 - 7.56 (m, 4 H) 7.27 - 7.35 (m, 1 H) 7.02 - 7.09 (m, 2 H). EI-HRMS: calcd for
27 C₂₂H₁₂O₂N₂ClFS [M]⁺: 422.02866; found: 422.02828; delta= -0.9 ppm. EI-MS m/z(rel int%): 422(100);
28 421(48); 387(13); 357(13); 323(10); 311(4); 279(10); 262(13); 251(8); 228(18); 201(14); 143(7); 95(8).
29
30

31 7-Chloro-4-(4-chlorophenyl)-3-((4-fluorophenyl)sulfonyl)quinoline (**20**): Mp: 194-196 °C. ¹H NMR (500
32 MHz, DMSO-*d*₆) δ ppm 9.65 (s, 1 H) 8.32 (d, *J*=2.2 Hz, 1 H) 7.69 (dd, *J*=9.1, 2.2 Hz, 1 H) 7.46 - 7.55 (m,
33 4 H) 7.26 - 7.34 (m, 3 H) 7.00 - 7.07 (m, 2 H). EI-HRMS: calcd for C₂₁H₁₂O₂NCl₂FS [M]⁺: 430.99443;
34 found: 430.99383; delta= -1.4 ppm. EI-MS m/z(rel int%): 431(100); 430(47); 366(10); 332(7); 320(4);
35 288(16); 272(7); 260(15); 237(21); 210(12); 201(11); 175(6); 174(6).
36
37
38
39
40
41
42
43
44
45
46
47
48
49
50
51
52
53
54
55
56
57
58
59
60

1
2
3 4-(4-Chlorophenyl)-3-((4-fluorophenyl)sulfonyl)quinoline-7-carbonitrile (**21**): Mp: 222 °C decomp. ¹H
4
5 NMR (500 MHz, DMSO-*d*₆) δ ppm 9.75 (s, 1 H) 8.72 - 8.93 (m, 1 H) 7.93 (dd, *J*=8.8, 1.6 Hz, 1 H) 7.52 -
6
7 7.57 (m, 2 H) 7.48 - 7.52 (m, 2 H) 7.42 (d, *J*=8.8 Hz, 1 H) 7.26 - 7.35 (m, 2 H) 7.02 - 7.10 (m, 2 H). EI-
8
9 HRMS: calcd for C₂₂H₁₂O₂N₂ClFS [M]⁺: 422.02866; found: 422.02767; delta= -2.3 ppm. EI-MS m/z(rel
10
11 int%): 422(100); 421(53); 357(15); 323(8); 311(5); 279(13); 263(7); 251(10); 228(16); 201(15); 143(9);
12
13 95(8).
14
15

16 6-Chloro-4-(4-chlorophenyl)-8-fluoro-3-((4-fluorophenyl)sulfonyl)quinoline (**22**): Mp: 198-199 °C. ¹H
17
18 NMR (500 MHz, DMSO-*d*₆) δ ppm 9.69 (s, 1 H) 8.11 (dd, *J*=10.0, 2.2 Hz, 1 H) 7.47 - 7.55 (m, 4 H) 7.27 -
19
20 7.36 (m, 2 H) 7.03 - 7.09 (m, 2 H) 7.01 (dd, *J*=2.1, 1.2 Hz, 1 H). EI-HRMS: calcd for C₂₁H₁₁O₂NCl₂F₂S [M]⁺:
21
22 448.98501; found: 448.98629; delta=2.8 ppm. EI-MS m/z(rel int%): 449(100); 448(32); 414(3); 384(8);
23
24 350(7); 306(7); 289(10); 278(8); 255(21); 228(4); 219(11); 193(4) 159(3); 143(6); 95(7).
25
26
27

28 3-((3-Chloro-4-fluorophenyl)sulfonyl)-7-fluoro-4-(4-fluorophenyl)quinoline (**23**): Mp: 176-177 °C. ¹H
29
30 NMR (500 MHz, DMSO-*d*₆) δ ppm 9.67 (s, 1 H) 8.03 (dd, *J*=9.8, 2.7 Hz, 1 H) 7.60 (ddd, *J*=9.4, 8.3, 2.7 Hz,
31
32 1 H) 7.46 - 7.57 (m, 2 H) 7.39 - 7.42 (m, 1 H) 7.37 (dd, *J*=9.3, 6.0 Hz, 1 H) 7.22 - 7.33 (m, 1 H) 7.02 - 7.12
33
34 (m, 2 H). EI-HRMS: calcd for C₂₁H₁₁O₂NClF₃S [M]⁺: 433.01456; found: 433.01367; delta= -2.1 ppm. EI-
35
36 MS m/z(rel int%): 433(100); 368(10); 333(13); 288(9); 256(22); 240(29); 228(20); 212(14); 193(8).
37
38
39

40 3-((7-Fluoro-4-(4-fluorophenyl)quinolin-3-yl)sulfonyl)benzonitrile (**24**): Mp: 182-183 °C. ¹H NMR (500
41
42 MHz, DMSO-*d*₆) δ ppm 9.68 (s, 1 H) 8.10 (dt, *J*=7.8, 1.3 Hz, 1 H) 8.04 (dd, *J*=9.9, 2.7 Hz, 1 H) 7.69 - 7.75
43
44 (m, 2 H) 7.62 - 7.67 (m, 1 H) 7.60 (ddd, *J*=9.4, 8.3, 2.7 Hz, 1 H) 7.36 (dd, *J*=9.3, 6.0 Hz, 1 H) 7.21 - 7.29
45
46 (m, 1 H) 6.99 - 7.08 (m, 2 H). EI-HRMS: calcd for C₂₂H₁₂O₂N₂F₂S [M]⁺: 406.05821; found: 406.05760;
47
48 delta= -1.5 ppm. EI-MS m/z(rel int%): 406(100); 341(22); 288(4); 256(13); 240(26); 228(13); 212(12);
49
50 193(7).
51
52

53 3-((4-(4-Chlorophenyl)-7-fluoroquinolin-3-yl)sulfonyl)benzonitrile (**25**): Mp: 209 °C. ¹H NMR (500 MHz,
54
55 DMSO-*d*₆) δ ppm 9.68 (s, 1 H) 8.11 (ddd, *J*=7.7, 1.4, 1.2 Hz, 1 H) 8.04 (dd, *J*=9.9, 2.6 Hz, 1 H) 7.73 - 7.78
56
57 (m, 2 H) 7.65 (td, *J*=7.8, 0.7 Hz, 1 H) 7.60 (ddd, *J*=9.3, 8.3, 2.7 Hz, 1 H) 7.43 - 7.50 (m, 2 H) 7.37 (dd,
58
59 *J*=9.3, 6.0 Hz, 1 H) 6.97 - 7.07 (m, 2 H). EI-HRMS: calcd for C₂₂H₁₂O₂N₂ClFS [M]⁺: 422.02866; found:
60

422.02781; δ = -2.0 ppm. EI-MS m/z (rel int%): 422(100); 387(3); 357(15); 323(6); 272(11); 256(14); 244(10); 221(24); 194(16).

3-((3,5-Dichlorophenyl)sulfonyl)-7-fluoro-4-(3-fluorophenyl)quinoline (26): Mp: 198-199 °C. ^1H NMR (500 MHz, $\text{DMSO}-d_6$) δ ppm 9.68 (s, 1 H) 8.05 (dd, $J=9.9, 2.6$ Hz, 1 H) 7.97 (t, $J=1.9$ Hz, 1 H) 7.57 - 7.67 (m, 1 H) 7.46 - 7.54 (m, 1 H) 7.39 - 7.45 (m, 2 H) 7.38 (d, $J=1.8$ Hz, 2 H) 6.88 - 6.98 (m, 2 H). EI-HRMS: calcd for $\text{C}_{21}\text{H}_{11}\text{O}_2\text{NCl}_2\text{F}_2\text{S}$ $[\text{M}]^+$: 448.98501; found: 448.98426; δ = -1.7 ppm. EI-MS m/z (rel int%): 449(100); 414(6); 384(14); 349(12); 288(10); 256(28); 240(43); 228(24); 212(17); 193(10).

3-((3,5-Difluorophenyl)sulfonyl)-7-fluoro-4-(4-fluorophenyl)quinoline (27): Mp: 162-164 °C. ^1H NMR (500 MHz, $\text{DMSO}-d_6$) δ ppm 9.65 (s, 1 H) 8.04 (dd, $J=9.9, 2.6$ Hz, 1 H) 7.53 - 7.71 (m, 2 H) 7.39 (dd, $J=9.3, 6.0$ Hz, 1 H) 7.22 - 7.30 (m, 1 H) 7.07 - 7.15 (m, 4 H). EI-HRMS: calcd for $\text{C}_{21}\text{H}_{11}\text{O}_2\text{NF}_4\text{S}$ $[\text{M}]^+$: 417.04411; found: 417.04397; δ = -0.3 ppm. EI-MS m/z (rel int%): 417(100); 416(32); 352(22); 288(5); 256(16); 240(32); 239(17); 228(16); 212(12); 193(7).

3-((3,5-Dichlorophenyl)sulfonyl)-8-fluoro-4-(4-fluorophenyl)quinoline (28): Mp: 189-191 °C. ^1H NMR (500 MHz, $\text{DMSO}-d_6$) δ ppm 9.69 (s, 1 H) 7.94 (t, $J=1.9$ Hz, 1 H) 7.87 (ddd, $J=10.6, 7.8, 1.0$ Hz, 1 H) 7.64 (td, $J=8.2, 5.1$ Hz, 1 H) 7.33 (d, $J=1.9$ Hz, 2 H) 7.24 - 7.31 (m, 1 H) 7.05 - 7.15 (m, 3 H). EI-HRMS: calcd for $\text{C}_{21}\text{H}_{11}\text{O}_2\text{NCl}_2\text{F}_2\text{S}$ $[\text{M}]^+$: 448.98501; found: 448.98676; δ =3.9 ppm. EI-MS m/z (rel int%): 449(100); 448(27); 414(4); 384(8); 350(6); 349(7); 288(6); 256(16); 240(30); 239(28); 228(17); 220(8); 212(10); 193(8).

8-Fluoro-4-(4-fluorophenyl)-3-((3-fluorophenyl)sulfonyl)quinoline (29): Mp: 123-124 °C. ^1H NMR (500 MHz, $\text{DMSO}-d_6$) δ ppm 9.69 (s, 1 H) 7.86 (ddd, $J=10.5, 7.7, 1.0$ Hz, 1 H) 7.64 (td, $J=8.2, 5.1$ Hz, 1 H) 7.47 - 7.56 (m, 2 H) 7.27 - 7.33 (m, 1 H) 7.20 - 7.27 (m, 1 H) 7.15 - 7.19 (m, 1 H) 7.11 (d, $J=8.6$ Hz, 1 H) 6.99 - 7.09 (m, 3 H). EI-HRMS: calcd for $\text{C}_{21}\text{H}_{12}\text{O}_2\text{NF}_3\text{S}$ $[\text{M}]^+$: 399.05354; found: 399.05255; δ = -2.5 ppm. EI-MS m/z (rel int%): 399(100); 334(17); 288(5); 256(12); 240(19); 239(19); 228(15); 220(5); 212(8); 193(5).

3-((3,5-Dichlorophenyl)sulfonyl)-7-fluoro-4-(4-fluorophenyl)quinoline (30): Mp: 182-184 °C. ^1H NMR (500 MHz, $\text{DMSO}-d_6$) δ ppm 9.66 (s, 1 H) 8.04 (dd, $J=9.8, 2.5$ Hz, 1 H) 7.94 (t, $J=1.8$ Hz, 1 H) 7.61 (td,

1
2
3 $J=8.8, 2.6$ Hz, 1 H) 7.39 (dd, $J=9.3, 6.0$ Hz, 1 H) 7.32 (d, $J=1.8$ Hz, 2 H) 7.24 - 7.31 (m, 2 H) 7.06 - 7.13
4
5 (m, 2 H). EI-HRMS: calcd for $C_{21}H_{11}O_2NCl_2F_2S$ $[M]^+$: 448.98501; found: 448.98467; $\delta=-0.8$ ppm. EI-
6
7 MS m/z (rel int%): 449(100); 448(38); 414(5); 384(10); 350(7); 349(10); 288(9); 256(24); 240(41);
8
9 239(24); 228(21); 220(5); 212(16); 193(9).

10
11 *3-((3,5-Difluorophenyl)sulfonyl)-7-fluoro-4-(3-fluorophenyl)quinoline (31)*: Mp: 170-171 °C. 1H NMR
12
13 (500 MHz, $DMSO-d_6$) δ ppm 9.66 (s, 1 H) 8.05 (dd, $J=9.8, 2.7$ Hz, 1 H) 7.66 (tt, $J=9.2, 2.2$ Hz, 1 H) 7.62
14
15 (ddd, $J=9.2, 8.4, 2.7$ Hz, 1 H) 7.48 (td, $J=8.0, 6.0$ Hz, 1 H) 7.35 - 7.44 (m, 2 H) 7.07 - 7.21 (m, 2 H) 6.86 -
16
17 7.00 (m, 2 H). EI-HRMS: calcd for $C_{21}H_{11}O_2NF_4S$ $[M]^+$: 417.04411; found: 417.04384; $\delta=-0.7$ ppm.
18
19 EI-MS m/z (rel int%): 417(100); 416(41); 352(27); 288(5); 256(17); 240(30); 239(18); 228(17); 212(11);
20
21 193(7).

22
23 *3-((3,4-Difluorophenyl)sulfonyl)-7-fluoro-4-(4-fluorophenyl)quinoline (32)*: Mp: 159-161 °C. 1H NMR
24
25 (500 MHz, $DMSO-d_6$) δ ppm 9.66 (s, 1 H) 8.03 (dd, $J=9.9, 2.6$ Hz, 1 H) 7.60 (ddd, $J=9.3, 8.4, 2.7$ Hz, 1 H)
26
27 7.51 - 7.58 (m, 1 H) 7.46 (ddd, $J=9.8, 7.4, 2.3$ Hz, 1 H) 7.37 (dd, $J=9.4, 6.0$ Hz, 1 H) 7.23 - 7.32 (m, 3 H)
28
29 7.05 - 7.12 (m, 2 H). EI-HRMS: calcd for $C_{21}H_{11}O_2NF_4S$ $[M]^+$: 417.04411; found: 417.04373; $\delta=-0.9$
30
31 ppm. EI-MS m/z (rel int%): 417(100); 416(47); 352(21); 288(8); 256(17); 240(25); 239(16); 228(17);
32
33 212(11); 193(6).

34
35 *3-((3-Chloro-4-fluorophenyl)sulfonyl)-4-(4-chlorophenyl)-7-fluoroquinoline (33)*: Mp: 143-144 °C. 1H
36
37 NMR (500 MHz, $DMSO-d_6$) δ ppm 9.67 (s, 1 H) 8.03 (dd, $J=9.9, 2.6$ Hz, 1 H) 7.60 (ddd, $J=9.4, 8.3, 2.7$ Hz,
38
39 1 H) 7.48 - 7.57 (m, 4 H) 7.39 (dd, $J=7.0, 2.2$ Hz, 1 H) 7.37 (dd, $J=9.3, 6.4$ Hz, 1 H) 7.02 - 7.09 (m, 2 H).
40
41 EI-HRMS: calcd for $C_{21}H_{11}O_2NCl_2F_2S$ $[M]^+$: 448.98501; found: 448.98643; $\delta=3.2$ ppm. EI-MS m/z (rel
42
43 int%): 449(100); 448(47); 384(8); 349(12); 272(21); 256(15); 244(17); 221(29); 194(20).
44
45

46
47 *3-((3,5-Difluorophenyl)sulfonyl)-8-fluoro-4-(4-fluorophenyl)quinoline (34)*: Mp: 177-179 °C. 1H NMR
48
49 (500 MHz, $DMSO-d_6$) δ ppm 9.68 (s, 1 H) 7.87 (ddd, $J=10.5, 7.8, 1.0$ Hz, 1 H) 7.58 - 7.71 (m, 2 H) 7.21 -
50
51 7.34 (m, 1 H) 7.08 - 7.16 (m, 6 H). EI-HRMS: calcd for $C_{21}H_{11}O_2NF_4S$ $[M]^+$: 417.04411; found:
52
53 417.04398; $\delta=-0.3$ ppm. EI-MS m/z (rel int%): 417(100); 416(24); 352(15); 288(3); 256(9); 240(23);
54
55 239(22); 228(13); 220(6); 212(7); 193(5).
56
57
58
59
60

1
2
3 4-(4-Chlorophenyl)-3-((3,5-dichlorophenyl)sulfonyl)-7-fluoroquinoline (**35**): Mp: 204 °C decomp. ¹H
4
5 NMR (500 MHz, DMSO-*d*₆) δ ppm 9.66 (s, 1 H) 8.05 (dd, *J*=9.9, 2.6 Hz, 1 H) 7.95 (t, *J*=1.9 Hz, 1 H) 7.60
6
7 (ddd, *J*=9.4, 8.4, 2.7 Hz, 1 H) 7.46 - 7.53 (m, 2 H) 7.39 (dd, *J*=9.3, 6.0 Hz, 1 H) 7.33 (d, *J*=1.8 Hz, 2 H)
8
9 7.02 - 7.11 (m, 2 H). EI-HRMS: calcd for C₂₁H₁₁O₂NCI₃FS [M]⁺: 464.95546; found: 464.95455; delta= -
10
11 2.0 ppm. EI-MS m/z(rel int%): 465(96); 400(8); 365(10); 272(31); 256(25); 244(20); 221(40); 194(27).
12
13

14 4-(4-Chlorophenyl)-3-((3,4-difluorophenyl)sulfonyl)-8-fluoroquinoline (**36**): Mp: 171-172 °C. ¹H NMR
15
16 (500 MHz, DMSO-*d*₆) δ ppm 9.68 (s, 1 H) 7.86 (ddd, *J*=10.6, 7.8, 1.1 Hz, 1 H) 7.64 (td, *J*=8.2, 5.1 Hz, 1
17
18 H) 7.56 (ddd, *J*=10.2, 8.7, 7.7 Hz, 1 H) 7.43 - 7.52 (m, 4 H) 7.32 - 7.38 (m, 1 H) 7.11 (d, *J*=8.5 Hz, 1 H)
19
20 7.02 - 7.09 (m, 2 H). EI-HRMS: calcd for C₂₁H₁₁O₂NCIF₃S [M]⁺: 433.01456; found: 433.01396; delta= -
21
22 1.4 ppm. EI-MS m/z(rel int%): 433(100); 432(30); 398(2); 368(11); 334(5); 304(3); 272(11); 256(11);
23
24 255(13); 244(12); 221(24); 194(10).
25
26
27

28 4-(4-Chlorophenyl)-3-((3,4-difluorophenyl)sulfonyl)-7-fluoroquinoline (**37**): Mp: 158-159 °C. ¹H NMR
29
30 (500 MHz, DMSO-*d*₆) δ ppm 9.65 (s, 1 H) 8.03 (dd, *J*=9.8, 2.7 Hz, 1 H) 7.60 (ddd, *J*=9.3, 8.4, 2.7 Hz, 2 H)
31
32 7.52 - 7.58 (m, 1 H) 7.48 - 7.53 (m, 2 H) 7.47 (ddd, *J*=9.3, 7.4, 2.2 Hz, 1 H) 7.37 (dd, *J*=9.3, 6.0 Hz, 1 H)
33
34 7.32 - 7.36 (m, 1 H) 7.00 - 7.13 (m, 2 H). EI-HRMS: calcd for C₂₁H₁₁O₂NCIF₃S [M]⁺: 433.01456; found:
35
36 433.01329; delta= -2.9 ppm. EI-MS m/z(rel int%): 433(100); 432(41); 398(1); 368(15); 334(6); 304(5);
37
38 272(16); 256(12); 244(14); 221(24); 194(16).
39
40
41
42
43
44

45 *Docking calculations* - The mGluR5-compound **1** complex structure (PDB code: 5CGC) was processed
46
47 by the protein preparation protocol of Schrödinger-Maestro v10.5.014 using default parameters. The
48
49 binding mode of **25** was investigated by Induced Fit Docking. A receptor grid box with the side length
50
51 of 20 Å and centered on the ligand was generated. The initial Glide docking was carried out with side
52
53 chains trimmed automatically based on B-factors, with receptor and ligand van der Waals scaling of
54
55 0.70 and 0.50, respectively generating 70 poses in total. Prime residue refinement and side chain
56
57 minimization were performed within 5.0 Å of ligand poses. Glide SP was used for redocking into the
58
59 top 50 receptor structures generated within 30 kcal/mol of the best structure as obtained from the
60

1
2
3 Prime refinement. The best scored mGluR5-25 complex structure was selected and the predicted
4
5 binding mode was analyzed.
6
7
8
9

10 *Binding hot spot projection on the mGluR5 binding site*

11
12 The identification of binding hot spot followed the previously described procedure.³² Group
13 efficiencies were used to identify binding hot spots and were calculated as follows: $GE = -\Delta\Delta G/\Delta N$,
14 where $\Delta\Delta G = \Delta G(\text{molecule B}) - \Delta G(\text{molecule A})$ and $\Delta N = HA(\text{molecule B}) - HA(\text{molecule A})$. To visualize
15 the GEs of the ligands on the protein surface non-hydrogen protein atoms within 4 Å distance of the
16 proposed binding mode of each non-hydrogen ligand atoms from were scored according to the GE.
17
18 The binding pocket surface was colored according to the maximum GE values for each protein atom.
19
20
21
22
23
24
25
26
27

28 *WaterFLAP calculations*

29
30 WaterFLAP was used as previously described.²⁶ Water networks of the solvated protein cavity were
31 optimized first in a short molecular dynamics simulation. The energies of the water molecules in the
32 resulting water network are then estimated by a GRID calculation³³ based on the OH2 (water) and
33 CRY (combining C1= and DRY) probes, and an entropy analysis of the degrees of freedom movement)
34
35 of the water molecules in the short molecular dynamics simulation.
36
37
38
39
40
41
42
43

44 **Pharmacology**

45
46 Manuscripts reporting data from experiments on live animals must include a statement identifying the
47 approving committee and certifying that such experiments were performed in accordance with all
48 national or local guidelines and regulations. Results from experiments involving humans or tissue
49 samples must additionally include a statement that informed consent was obtained from the subject
50 or from the next of kin.
51
52
53
54
55
56
57
58
59
60

1
2
3 *Rat cortical and human recombinant mGlu5 binding assay (rat and human mGluR5 binding)* - The
4
5 mGluR5 receptor binding was determined according to Gasparini et al.²⁹ with modifications. Rat
6
7 cerebrocortical membrane preparation was used to determine the binding characteristics of reference
8
9 compounds and novel compounds to the rat mGluR5. The A18 cell line recombinantly expressing
10
11 hmGluR5a (purchased from Euroscreen) was used to determine binding characteristics of the chemical
12
13 compounds to the human mGluR5 receptor. The non-specific binding was determined in the presence
14
15 of 10 mM M-MPEP. Assays were carried out in 96-well format, the rat cortical membrane homogenates
16
17 or membrane homogenates of A18 hmGluR5 cells were incubated in binding buffer (50 mM Tris buffer
18
19 (pH: 7.6) supplemented with 2 mM MgCl₂, 2 mM CaCl₂) in the presence of radioligand [³H]M-MPEP and
20
21 drugs under investigation in a total volume of 0.3 ml for 60 minutes at 25°C. The radioligand
22
23 displacement by the tested compounds was determined in duplicates or triplicates. For IC₅₀ (K_i)
24
25 determinations concentration–displacement curves were generated consisting of generally 7
26
27 concentrations. K_i values (i.e., inhibition constants) were calculated using the Cheng–Prusoff equation:
28
29 $K_i = IC_{50}/[1 + (L/K_d)]$, where [L] is the radioligand concentration and K_d the affinity of the labeled ligand
30
31 for receptor. K_d was determined from the Scatchard plot.
32
33
34
35
36
37
38
39

40 *Rat, dog and human liver microsomal stability assay* - In vitro metabolic stability was assessed using
41
42 human (Xenotech, USA), dog (Xenotech, USA) and Wistar rat (In Vitro Metabolism Research, Gedeon
43
44 Richter Plc, Hungary) liver microsomes. Test compounds at 2.5 μM initial test concentration were
45
46 incubated for various length of time with the liver microsomes (0.5 mg/mL). In vitro intrinsic clearance
47
48 (Cl_{int} mL/min*g liver) was calculated using the basic concept of clearance prediction³⁴ according to
49
50 following equations: Cl_{int}=V_{max}/K_M or if S<<K_M Cl_{int}=V/S; V_{max}= maximal rate of enzyme reaction; K_M=
51
52 affinity constant of substrate concentration; V=actual rate of enzyme reaction under first order
53
54 conditions.
55
56
57
58
59
60

1
2
3 *Assessment of functional activity at human mGluR5 receptors (human mGluR5 functional)* - Cell
4
5 culturing: Chinese hamster ovary (CHO) cells stably expressing recombinant human mGluR5a (CHO-
6
7 mGluR5a) receptors were maintained in F12 medium containing 10% FCS, 1% antibiotic antimycotic
8
9 solution, 400 µg/ml G418, 250 µg/ml zeocin, 5 µg/ml puromycin. For the Ca²⁺ measurements cells were
10
11 plated at 2.5-3.5×10⁴ cell/well on standard 96-well microplates, receptor expression was induced by
12
13 adding 1350 nM doxycycline on the next day. Fluorometric calcium measurements were carried out
14
15 16-24 hours after the addition of the inducing agent.

16
17
18
19 Fluorimetric measurement of cytosolic calcium concentration: Before the measurement cells were
20
21 loaded with a fluorescent Ca²⁺-sensitive dye, fluo-4/AM (2 µM) in assay buffer (145 mM NaCl, 5 mM
22
23 KCl, 2 mM MgCl₂, 2 mM CaCl₂, 10 mM HEPES, 20 mM D-glucose, 2 mM probenecid, 2 mM Na-pyruvate,
24
25 30 µg/ml glutamate-pyruvate transaminase, pH=7.4). Dye loading was done by incubating the cells
26
27 with 100 µl/well dye solution at 37 °C for 40-120 min. To stop dye loading cells were washed twice
28
29 with assay buffer. After washing, various concentrations of the test compounds (diluted in assay buffer
30
31 from a DMSO or a dimethylformamide (DMF) stock solution, final DMSO/DMF concentration was
32
33 <0.1%) or buffer were added to each well depending on the experimental setup. After incubation at
34
35 37 °C for 10-20 min. baseline and agonist-evoked changes of [Ca²⁺]_i were measured column by column
36
37 with a plate reader fluorimeter (FlexStation II, Molecular Devices). Excitation and detection of emission
38
39 was carried out from the bottom of the plate. The whole measurement process was performed at 37
40
41 °C and was controlled by custom software (SoftMax Pro, Molecular Devices). Inhibitory potency of the
42
43 test compounds was assessed by measuring the reduction in the agonist-evoked [Ca²⁺]_i-elevation in
44
45 the presence of different concentrations of the compounds. DHPG (20 µM) was used as agonist.
46
47 Fluorescence data were expressed as ΔF/F (fluorescence change normalized to baseline) values. All
48
49 treatments on a single plate were measured in multiple wells. Data from all wells with the same
50
51 treatment were averaged and the average values were used for analysis. Inhibitory potency of a
52
53 compound at a single concentration point was expressed as percent inhibition of the control agonist
54
55 response. Sigmoidal concentration-inhibition curves were fitted to the data (derived from at least
56
57
58
59
60

1
2
3 three independent experiments) and IC50-values were determined as the concentration that produces
4
5 half of the maximal inhibition caused by the compound. Data were analyzed using SoftMax Pro
6
7 (Molecular Devices).
8
9

10 11 12 *Vogel punished drinking conflict test in rats*

13
14 The method uses a conflict situation created by the simultaneous presence of attractive and aversive
15
16 stimuli as a model of anxiety state.³⁵ On the preceding day of the test rats are placed into the test
17
18 chambers equipped with a metal water spout mounted on the wall of the chamber and a metal grid
19
20 floor for delivering electric shocks. During a 5-min adaptation period they have free access to the
21
22 drinking spout. Following the adaptation session animals are deprived of drinking water for 24h prior
23
24 to test. On the day of the measurement, the animals are treated with the test compounds then placed
25
26 into the test chambers where they have free access to drinking water for a 60-s unpunished period.
27
28 After that, electric shocks (1mA, 1 sec) are applied through the drinking spout following every 10 licks
29
30 during a 270-s punished period. Number of licks and shocks delivered are recorded and stored in a
31
32 computer. Anxiolytic or anxiogenic activity is reflected by increased or decreased number of accepted
33
34 shocks, respectively.
35
36
37
38
39
40
41

42 *Morris water maze*

43
44 Apparatus - The Morris water maze consisted of a circular pool with black walls, 2 m in diameter and
45
46 0.60 m in height. The pool was filled with water (25 ± 1 °C) to a depth of 45 cm. The pool was divided
47
48 to four imaginary quadrants by two perpendicular diameters. The points at which they sectioned the
49
50 perimeter of the pool were arbitrarily named as north (N), east (E), south (S) and west (W). These
51
52 points served as the "start" positions of the animals. A circular escape platform (10 cm diameter) with
53
54 its top surface hidden 2 cm beneath the water was placed in the middle of the southeast quadrant of
55
56 the pool. A video camera placed 1.40 m above the center point of the maze monitored the behavior
57
58 of the rats in the pool and the video signal was transmitted to a computer controlled motion tracking
59
60

1
2
3 and analyzer system. The image analyzer transformed the conventional video image to a digitized
4
5 image with x and y coordinates of the white-black edges on the rat's head. The digitized signal was
6
7 stored and analyzed by software (Poly-Track, San Diego Instruments). The program determined the
8
9 path swum by the rats, times spent by them in predefined zones of the pool and latency to find the
10
11 platform. It also calculated the distance and speed of swimming. The test room contained several
12
13 permanent extra maze cues which helped the animals to navigate in the pool.
14
15

16
17 Procedure- The compound was investigated in two studies and the data obtained in the separated
18
19 experiments were summarized (7-17 rats/groups). The experiments included a solvent control and
20
21 drug-treated groups. Following administration of the compound or vehicle, the animals were
22
23 individually placed into the pool. The rats (adult male Harlan-Wistar rats weighing 190-220 g) were
24
25 given three training trials a day, over 4 consecutive days. At least 20 min rest periods were allowed
26
27 between trials. In each trial the rat was placed in the maze at one of the four start positions. Each day
28
29 the start positions were randomized for each animal, across trials, so that all four start positions were
30
31 used. Escape latency and distance travelled were recorded. If the rat did not locate the platform within
32
33 120 sec, the animal was gently guided to the platform by hand. In this case the swimming time was
34
35 recorded as the maximum 120 sec. Every rat was allowed to remain on the platform undisturbed for a
36
37 total of 20 sec.
38
39
40
41
42
43

44 45 **Corresponding author information**

46
47 For G.M.K.: gy.keseru@ttk.mta.hu

48
49 For G.D.: gy.domany@richter.hu

50 51 52 53 **Acknowledgement**

54
55 The authors are grateful to Aaron Keeley (RCNS, Hungary) carefully reading the manuscript and
56
57 Gabriele Cruciani (Molecular Discovery, UK) for granting a WaterFLAP license. The support of the
58
59 National Brain Research Program (KTIA_NAP_13-1-2013-0001) is acknowledged.
60

Abbreviations used

DHPG, (S)-3,5-dihydroxyphenylglycine; GE, group efficiency; HPMC, (Hydroxypropyl)methyl cellulose; PDR, permeability directional ratio.

References

- 1 Nakanishi, S. Molecular diversity of glutamate receptors and implications for brain function. *Science* **1992**, *258*, 597–603.
- 2 Bailey, D.B.; Berry-Kravis, E.; Wheeler, A.; Raspa, M.; Merrien, F.; Ricart, J.; Koumaras, B.; Rosenkranz, G.; Tomlinson, M.; von Raison, F.; Apostol, G. Mavoglurant in adolescents with fragile X syndrome: analysis of clinical global impression-improvement source data from a double-blind therapeutic study followed by an open-label, long-term extension study. *J. Neurodev. Disord.* **2016**, *8*, 1.
- 3 Pecknold, J. C.; McClure, D. J.; Appeltauer, L.; Wrzesinski, L.; Allan, T. Treatment of anxiety using fenobam (a nonbenzodiazepine) in a double-blind standard (diazepam) placebo-controlled study. *J. Clin. Psychopharmacol.* **1982**, *2*, 129–133.
- 4 Quiroz, J. A.; Tamburri, P.; Deptula, D.; Banken, L.; Beyer, U.; Fontoura, P.; Santarelli, L. The efficacy and safety of basimglurant as adjunctive therapy in major depression; a randomised, double-blind, placebo-controlled study. *Eur. Neuropsychopharmacol.* **2014**, *24*, S468.
- 5 Conn, P. J.; Lindsley, C. W.; Jones, C. K. Activation of metabotropic glutamate receptors as a novel approach for the treatment of schizophrenia. *Trends Pharmacol. Sci.* **2009**, *30*, 25–31.
- 6 Balschun, D.; Zuschratter, W.; Wetzell, W. Allosteric enhancement of metabotropic glutamate receptor 5 function promotes spatial memory. *Neuroscience* **2006**, *142*, 691–702.
- 7 Stefani, M.R.; Moghaddam, B. Activation of type 5 metabotropic glutamate receptors attenuates deficits in cognitive flexibility induced by NMDA receptor blockade. *Eur. J. Pharmacol.* **2010**, *639*, 26–32.

- 1
2
3
4
5 8 Lindsley, C. W.; Emmitte, K. A.; Hopkins, C. R.; Bridges, T. M.; Gregory, K. J.; Niswender, C. M.;
6
7 Conn, P. J. Practical strategies and concepts in GPCR allosteric modulator discovery: recent
8
9 advances with metabotropic glutamate receptors. *Chem. Rev.* **2016**, *116*, 6707-6741.
10
11 9 Keyword, C.; Wakefield, M.; Tack, J. A proof-of-concept study evaluating the effect of ADX10059, a
12
13 metabotropic glutamate receptor-5 negative allosteric modulator, on acid exposure and symptoms in
14
15 gastro-oesophageal reflux disease. *Gut* **2009**, *58*, 1192-1199.
16
17
18 10 Jaeschke, G.; Kolczewski, S.; Spooren, W.; Vieira, E.; Bitter-Stoll, N.; Boissin, P.; Borroni, E.;
19
20 Büttelmann, B.; Ceccarelli, S.; Clemann, N.; David, B.; Funk, C.; Guba, W.; Harrison, A.; Hartung, T.;
21
22 Honer, M.; Huwyler, J.; Kuratli, M.; Niederhauser, U.; Pahler, A.; Peters, J.-U.; Petersen, A.; Prinssen,
23
24 E.; Ricci, A.; Rueher, D.; Rueher, M.; Schneider, M.; Spurr, P.; Stoll, T.; Tannler, D.; Wichmann, J.;
25
26 Porter, R. H.; Wettstein, J. G.; Lindemann, L. Metabotropic glutamate receptor 5 negative allosteric
27
28 modulators: discovery of 2-chloro-4-[1-(4-fluorophenyl)-2,5-dimethyl-1H-imidazol-4-
29
30 ylethynyl]pyridine (basimglurant, RO4917523), a promising novel medicine for psychiatric diseases. *J.*
31
32 *Med. Chem.* **2015**, *58*, 1358-1371.
33
34
35 11 Vranesic, I.; Ofner, S.; Flor, P. J.; Bilbe, G.; Bouhelal, R.; Enz, A.; Desrayaud, S.; McAllister, K.; Kuhn,
36
37 R.; Gasparini, F. AFQ056/ mavoglurant, a novel clinically effective mGluR5 antagonist: identification,
38
39 SAR and pharmacological characterization. *Bioorg. Med. Chem.* **2014**, *22*, 5790-5803.
40
41
42 12 Tison, F.; Keyword, C.; Wakefield, M.; Durif, F.; Corvol, J.-C.; Eggert, K.; Lew, M.; Isaacson, S.; Bezard,
43
44 E.; Poli, S.-M.; Goetz, C. G.; Trenkwalder, C.; Rascol, O. A Phase 2A Trial of the Novel mGluR5-Negative
45
46 Allosteric Modulator Dipraglurant for Levodopa-Induced Dyskinesia in Parkinson's Disease. *Mov.*
47
48 *Disord.* **2016**, *31*, 1373-1380.
49
50
51 13 Raboisson, P.; Breitholtz-Emanuelsson, A.; Dahllöf, H.; Edwards, L.; Heaton, W. L.; Isaac, M.; Jarvie,
52
53 K.; Kers, A.; Minidis, A. B.; Nordmark, A.; Sheehan, S. M.; Slassi, A.; Ström, P.; Terelius, Y.; Wensbo, D.;
54
55 Wilson, J. M.; Xin, T.; McLeod, D. A. Discovery and characterization of AZD9272 and AZD6538-Two
56
57 novel mGluR5 negative allosteric modulators selected for clinical development. *Bioorg. Med. Chem.*
58
59 *Lett.* **2012**, *22*, 6974-6979.
60

- 1
2
3
4
5 14 Christopher, J. A.; Aves, S. J.; Bennett, K. A.; Doré, A. S.; Errey, J. C.; Jazayeri, A.; Marshall, F. H.;
6
7 Okrasa, K.; Serrano-Vega, M. J.; Tehan, B. G.; Wiggin, G. R.; Congreve, M. Fragment and structure-
8
9 based drug discovery for a class C GPCR: discovery of the mGlu5 negative allosteric modulator
10
11 HTL14242 (3-chloroc-5-[6-(5-fluoropyridin-2-yl)pyrimidin-4-yl]benzotrile). *J. Med. Chem.* **2015**, *58*,
12
13 6653-6664.
14
15
16 15 Galambos, J.; Domány, G.; Nógrádi, K.; Wágner, G.; Keserű, G. M.; Bobok, A.; Kolok, S.; Mikó-Bakk,
17
18 M. L.; Vastag, M.; Sághy, K.; Kóti, J.; Szakács, Z.; Béni, Z.; Gál, K.; Szombathelyi, Z.; Greiner, I. 4-Aryl-3-
19
20 arylsulfonyl-quinolines as negative allosteric modulators of metabotropic GluR5 receptors: from HTS
21
22 hit to development. *Bioorg. Med. Chem. Lett.* **2016**, *24*, 1249-1252.
23
24
25 16 Nógrádi, K.; Wágner, G.; Domány, G.; Bobok, A.; Magdó, I.; Kiss, B.; Kolok, S.; Fónagy, K.; Gyertyán,
26
27 I.; Háda, V.; Kóti, J.; Gál, K.; Farkas, S.; Keserű, G. M.; Greiner, I.; Szombathelyi, Z. Thieno[2,3-
28
29 b]pyridines as negative allosteric modulators of metabotropic GluR5 receptors: hit-to-lead
30
31 optimization. *Bioorg. Med. Chem. Lett.* **2014**, *24*, 3845-3849.
32
33
34 17 Nógrádi, K.; Wágner, G.; Domány, G.; Bobok, A.; Magdó, I.; Kolok, S.; Mikó-Bakk, M. L.; Vastag,
35
36 M.; Sághy, K.; Gyertyán, I.; Kóti, J.; Gál, K.; Farkas, S.; Keserű, G. M.; Greiner, I.; Szombathelyi, Z.
37
38 Thieno[2,3-b]pyridines as negative allosteric modulators of metabotropic GluR5 receptors: lead
39
40 optimization. *Bioorg. Med. Chem. Lett.* **2015**, *25*, 1724-1729.
41
42
43 18 Conn, P. J.; Christopoulos, A.; Lindsley, C. W. Allosteric modulation of GPCRs as a novel approach
44
45 to treatment of CNS disorders. *Nat. Rev. Drug Discovery* **2009**, *8*, 41-54.
46
47
48 19 Wood, M. R.; Hopkins, C. R.; Brogan, J. T.; Conn, P. J.; Lindsley, C. W. "Molecular switch" on
49
50 mGluR allosteric ligands that modulate modes of pharmacology. *Biochemistry* **2011**, *50*, 2403-2410.
51
52
53 20 Gentry, P. R.; Kokubo, M.; Bridges, T. M.; Kett, N. R.; Harp, J. M.; Cho, H. P.; Smith, E.; Chase, P.;
54
55 Hodder, P. S.; Niswender, C. M.; Daniels, J. S.; Conn, P. J.; Wood, M. R.; Lindsley, C. W. Discovery of
56
57 the first M5-selective and CNS penetrant negative allosteric modulator (NAM) of a muscarinic
58
59 acetylcholine receptor: (S)-9b-(4-chlorophenyl)-1-(3,4-difluorobenzoyl)-2,3-dihydro-1H-imidazo[2,1-
60
a]isoindol-5(9bH)-one (ML375), an M5 selective NAM. *J. Med. Chem.* **2013**, *56*, 9351-9355.

- 1
2
3
4
5 21 Kurata, H.; Gentry, P. R.; Kokubo, M.; Cho, H. P.; Bridges, T. M.; Niswender, C. M.; Byers, F. W.;
6
7 Wood, M. R.; Daniels, J. S.; Conn, P. J.; Lindsley, C. W. Further optimization of the M5 NAM MLPCN
8
9 probe ML375: tactics and challenges. *Bioorg. Med. Chem. Lett.* **2015**, *25*, 690–694.
10
11 22 Rydberg, P.; Gloriam, D. E.; Olsen, L. The SmartCyp cytochrome P450 metabolism prediction
12
13 server. *Bioinformatics*, **2010**, *26*, 2988-2989.
14
15 23 Conn, P. J.; Lindsley, C. W.; Meiler, J.; Niswender, C. M. Opportunities and challenges in the
16
17 discovery of allosteric modulators of GPCRs for treating CNS disorders. *Nat. Rev. Drug Discovery*
18
19 **2014**, *13*, 692–708.
20
21 24 Gasparini, F.; Lingenhohl, K.; Stoehr, N.; Flor, P. J.; Heinrich, M.; Vranesic, I.; Biollaz, M.; Allgeier,
22
23 H.; Heckendorn, R.; Urwyler, S.; Varney, M. A.; Johnson, E. C.; Hess, S. D.; Sacaan, A. I.;
24
25 Santori, E. M.; Velicelebi, G.; Kuhn, R. 2-Methyl-6-(phenylethynyl)-pyridine (MPEP), a potent,
26
27 selective and systemically active mGluR5 receptor antagonist. *Neuropharmacology* **1999**, *38*,
28
29 1493–1503.
30
31 25 Ballesteros, J. A.; Weinstein, H. Integrated methods for the construction of three-dimensional
32
33 models and computational probing of structure-function relations in G protein-coupled receptors.
34
35 *Methods Neurosci.* **1995**, *25*, 366–428.
36
37 26 Mason, J. S.; Bortolato, A.; Weiss, D. R.; Deflorian, F.; Tehan, B.; Marshall, F. High end GPCR
38
39 design: crafted ligand design and druggability analysis using protein structure, lipophilic hotspots and
40
41 explicit water networks. *In Silico Pharmacol.* **2013**, *1*, 23.
42
43 27 Verdonk, M. L.; Rees, D. C. Group efficiency: a guideline for hits-to-leads chemistry.
44
45 *ChemMedChem* **2008**, *3*, 1179–1180.
46
47 28 Kasper Harpsøe, K.; Isberg, V.; Tehan, B. G.; Weiss, D.; Arsova, A.; Marshall, F. H.; Bräuner-
48
49 Osborne, H.; Gloriam, D. E. Selective negative allosteric modulation of metabotropic glutamate
50
51 receptors – A structural perspective of ligands and mutants. *Sci. Rep.* **2015**, *5*, 13869.
52
53 29 Gasparini, F.; Andres, H.; Flor, P.J.; Heinrich, M.; Inderbitzin, M.; Lingenhöhl, K.; Müller, H.; Munk,
54
55 V. C.; Omilusik, K.; Stierlin, C.; Stoehr, N.; Vranesic, I.; Kuhn, R. [³H]-M-MPEP, a potent, subtype-
56
57
58
59
60

1
2
3
4
5 selective radioligand for the metabotropic glutamate receptor subtype 5. *Bioorg. Med. Chem.*
6
7 *Lett.* **2002**, *12*, 407– 409.

8
9 30 Lavreysen, H.; Janssen, C.; Bischoff, F.; Langlois, X.; Leysen, J. E.; Lesage, A. S. 3HR214127: a novel
10
11 high-affinity radioligand for the mGlu1 receptor reveals a common binding site shared by multiple
12
13 allosteric antagonists. *Mol. Pharm.* **2003**, *63*, 1082-1093.

14
15
16 31 Pouton C. W. Formulation of poorly water-soluble drugs for oral administration: Physicochemical
17
18 and physiological issues and the lipid formulation classification system. *Eur. J. Pharm. Sci.* **2006**, *29*,
19
20 278-287.

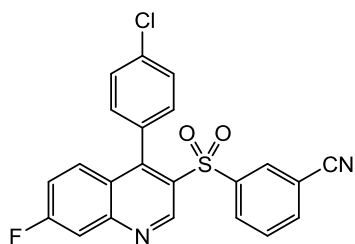
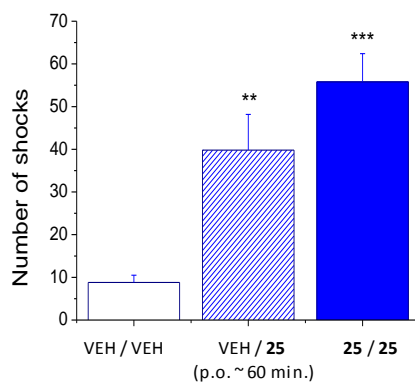
21
22
23 32 Kuhne, S.; Kooistra, A. J.; Bosma, R.; Bortolato, A.; Wijnmans, M.; Vischer, H. F.; Mason, J. S.; de
24
25 Graaf, C.; de Esch, I. J.; Leurs, R. Identification of ligand binding hot spots of the histamine H1
26
27 receptor following structure-based fragment optimization. *J. Med. Chem.* **2016**, *59*, 9047-9061.

28
29
30 33 Goodford, P. J. A computational procedure for determining energetically favorable binding sites
31
32 on biologically important macromolecules. *J. Med. Chem.* **1985**, *28*, 849–857.

33
34 34 Rane, A.; Wilkinson, G. R.; Shand, D. G. Prediction of hepatic extraction ratio from in vitro
35
36 measurement of intrinsic clearance. *J. Pharmacol. Exp. Ther.* **1977**, *200*, 420-424.

37
38
39 35 Vogel, J. R.; Beer, B.; Clody, D. E. A simple and reliable conflict procedure for testing anti-anxiety
40
41 agents. *Psychopharmacology* **1971**, *100*, 138-140.

Table of Contents graphic

**25**mGluR5 K_i = 4.9 nMmGluR5 IC_{50} = 13 nM*Vogel punished drinking conflict test (rat)*

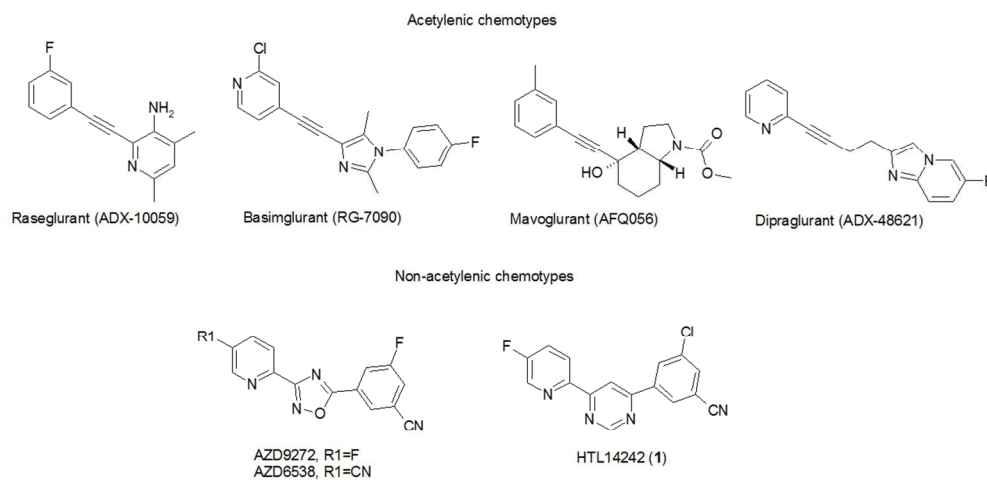


Figure 1

338x190mm (96 x 96 DPI)

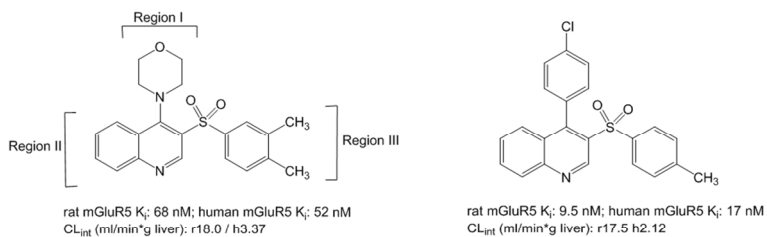


Figure 2

338x190mm (96 x 96 DPI)

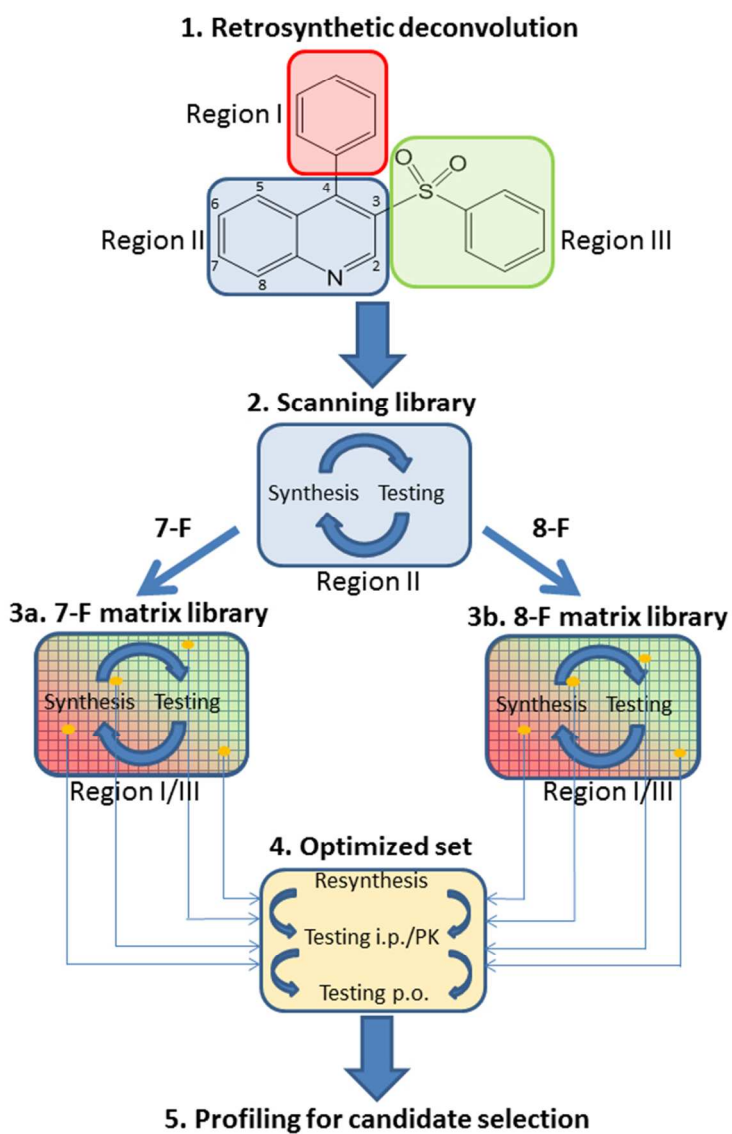
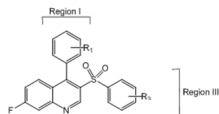


Figure 3

190x254mm (96 x 96 DPI)

Matrix library of 7-fluoroquinoline derivatives



Intrinsic clearance, human (ml/min*g liver)

Region III

Region I	Region III											average		
Region I	2-F	3-F	4-F	3-CN	3-OMe	4-OMe	3,4-Me2	3,4-F2	3,5-Cl2	3,5-F2	3-Cl,4-F	3-Cl,4-OMe	3,4,4-Me	average
2-F				1.39				0.79	0.93		1.07			1.05
3-F	0.24	0.95	0.76	3.36	2.94	3.71	0.60	0.41	0.06	0.25	2.08	0.41		1.32
4-F	0.11	1.34	0.39	9.37	1.71	9.25	0.44	0.18	0.01	0.69	1.29	2.33		2.26
3-Cl			0.99	2.97		4.01	0.38	0.93	0.22	0.66	1.19	2.13		1.50
4-Cl	0.98	1.25	0.31		1.28	7.88	0.01	0.13	0.03	0.39				1.36
3-OMe				1.83		8.78	1.77	1.51	1.81		1.71			2.90
4-OMe	1.89	1.77	0.92		1.18	4.13	1.10	1.00	1.51	1.08				1.62
average	0.81	1.33	0.94	5.23	1.78	6.29	0.73	0.73	0.61	0.69	1.57	1.62		

Figure 4a

338x190mm (96 x 96 DPI)

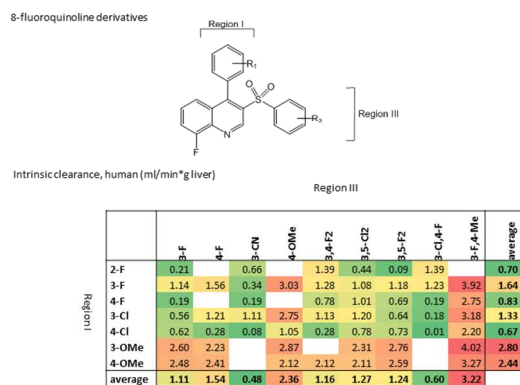


Figure 4b

338x190mm (96 x 96 DPI)

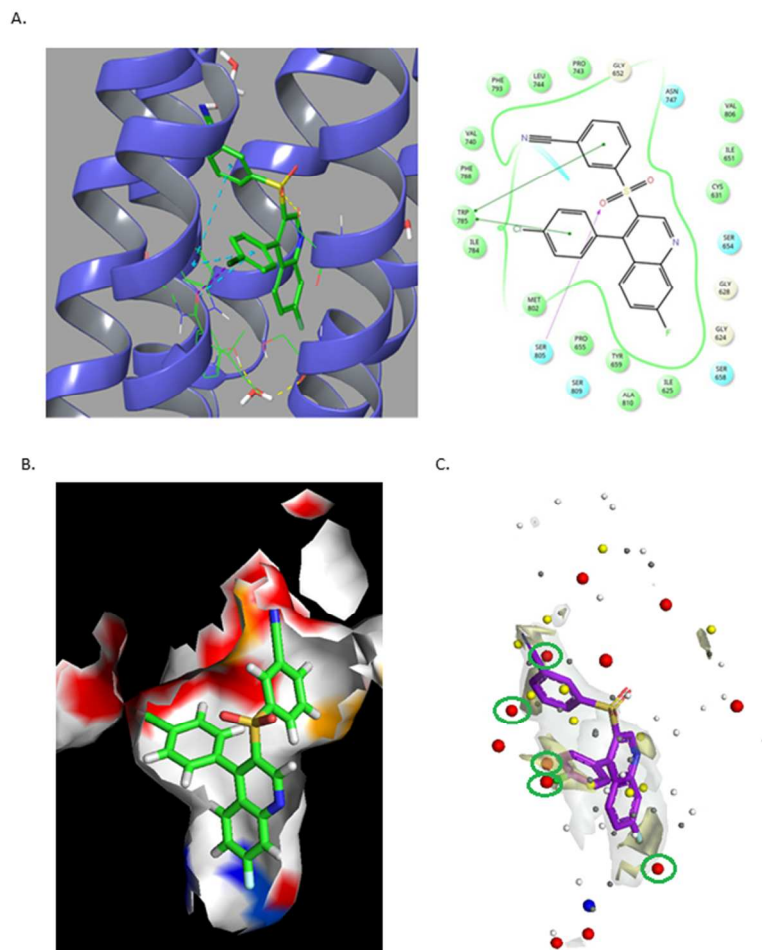


Figure 5

190x254mm (96 x 96 DPI)

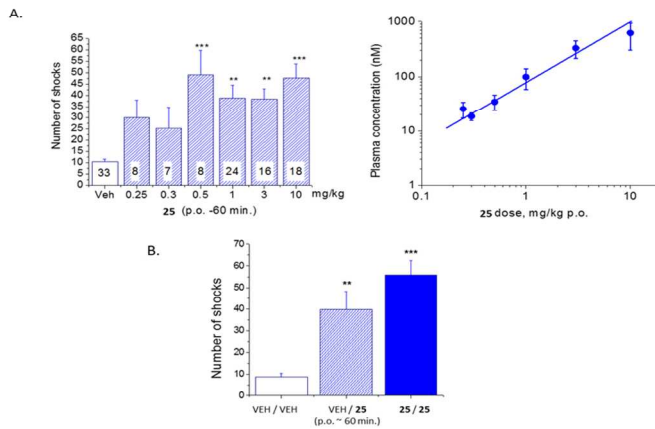


Figure 6

338x190mm (96 x 96 DPI)